

https://dspace.org/

Modelling the Inhomogeneities of the extragalactic background light

Kudoda, Ayman Mohamed ELhadi Mohamed

2016
http://hdl.handle.net/10539/19295

Downloaded from a DSpace repository. https://dspace.org/



Modelling the Inhomogeneities of the Extragalactic Background Light

Ayman Mohamed ELhadi Mohamed Kudoda

A Dissertation Submitted to the
Faculty of Science, University of the Witwatersrand, Johannesburg,
in Fulfillment of the Requirements for the Degree of
Master of Science.

August 2015

Declaration

I Ayman Mohamed Elhadi Modhamed Kudoda (Student number:949916) am a student registered for Master of Science in the year 2014 under the supervision of Dr. Andreas Faltenbacher. I hereby declare the following:

- I am aware of what plagiarism entails and the University's policy in this regard.
- This thesis work has not been submitted in support of an application for another degree or examination at any other University.
- This thesis is my own, original work. Where someone elses work was used (whether from a printed source, the internet or any other source) due acknowledgement was given and reference was made according to departmental requirements.
- I have followed the required conventions in referencing the thoughts and ideas of others.

Signature: _____ Date: 04/08/2015

Abstract

This work investigates the impact of the extragalactic background light fluctuations on very high energy γ-ray spectra from distant blazars. We calculate the extragalactic background light spectral energy distribution using a model that extends those proposed by Razzaque et al. (2009ApJ.697.483R) and Finke et al. (2010ApJ.712.238F). We introduce a model for fluctuations in the extragalactic background light based on fluctuations in the star formation rate density, since these two fluctuations can reasonably be expected to be correlated. Fluctuations in the star formation rate are estimated from the semi-analytical galaxy catalogue of Guo et al. (2013MNRAS.428.1351G), we use his model to derive the resulting opacities for γ-rays from distant sources. We determine the mean, lower and upper limits for the scatter of the star formation rate density, which then allow us to compute corresponding limits on the extragalactic background light spectrum. We then calculate the impact of these fluctuations limits on the γ-ray optical depth. This appears to be the first detailed analytical model that aims to account for the impact of extragalactic background light fluctuations on the γ-ray opacity. The model predicts relatively high variations ($\leq 15\%$) on the opacity in the energy range less than 100 GeV for nearby sources. The impact is found to be smaller ($\sim 5\%$) for very high energy γ-rays from distant sources.

Dedication

I dedicate this work to my family. To my mother, Fatma Ali, whose love, support and guidance kept me focused and motivated. She made it her top priority to see me achieve my goal of completing this Masters Degree. To my three brothers, Ashraf, Ahmed and Khalid, who encouraged me during my late nights of research and writing. And finally, to my late father, Mohamed Elhadi, who planted in me the yearning for knowledge and science from an early age.

Ayman.

Acknowledgment

I am grateful to my supervisor, Dr. A. Faltenbacher, who spent a considerable amount of time guiding the myriad aspects of this project. I could not have done it without his constant encouragement throughout this work, and his exceptional patience with the editing and re-editing of my work, when a lesser mortal could have gone insane. Above all, he was instrumental in developing and conceptualizing the idea behind this research.

I want to extend my gratitude and appreciationton to my friend Dr. Nebiha Shafi, who was the best editor and spell-checker I could have asked for. My thanks and appreciation to Dr. Asadig Mohammed and Dr. Ihab F. Riad for comments that greatly improved the manuscript.

This research was supported by the National Astrophysics and Sapce Science Programme (NASSP). The Millennium Simulation (MR7) databases used in this paper and the web application providing online access to them were constructed as part of the activities of the German Astrophysical Virtual Observatory (GAVO).

And I would be remiss if I failed to acknowledge my many relatives and countless friends who stood behind me along this journey.

Contents

Declaration ii

Abstract iii

Dedication iv

Acknowledgment v

List of Physical Constants and Symbols xi

List of Abbreviations xii

1 Introduction 1
- 1.1 Background . . . 1
- 1.2 Problem Statement . . . 3
- 1.3 Aims . . . 3
- 1.4 Outline . . . 3

2 Literature Review 4
- 2.1 Extragalacitc Background Light . . . 4
  - 2.1.1 Definition of the EBL . . . 4
  - 2.1.2 Contributors of the EBL . . . 5
  - 2.1.3 Measurements of the EBL . . . 7
  - 2.1.4 EBL Density . . . 8
  - 2.1.5 Models of the EBL . . . 9
- 2.2 Gamma-ray Astrophysics . . . 14
  - 2.2.1 Gamma-ray Emission Mechanisms . . . 14
  - 2.2.2 Sources of GeV/TeV Gamma-ray Emission . . . 16
  - 2.2.3 Interaction of Gamma-rays with Matter . . . 17
  - 2.2.4 Interaction of Gamma-rays with Electromagnetic Spectrum . . . 19
  - 2.2.5 Gamma-ray Detection . . . 20

3 A New Model for EBL 22
- 3.1 Razzaque Model . . . 22
- 3.2 Finke Model . . . 27
- 3.3 Numerical Implementation . . . 28

4 Results **34**
4.1 Fluctuations in the Star Formation History 34
4.2 Upper and Lower Limits of the EBL Density 36
4.3 Upper and lower Limits of Gamma-ray Opacity 36

5 Conclusions **40**

Bibliography **41**

List of Figures

2.1 The predicted EBL spectrum displayed as black line compared with observations, from Primack *et al.* (2005). 5
2.2 The evolution of the EBL with redshift proposed by (Primack *et al.* , 2005). 6
2.3 Different Backward Evolution models predicting the EBL spectrum, adapted from Hauser & Dwek (2001). 10
2.4 Comparison between predictions of different FE models and the observed EBL spectrum, adapted from Hauser & Dwek (2001). . 11
2.5 Comparison between the predictions of different cosmic chemical evolution and semi-analytical models and the observed EBL spectrum, adapted from Hauser & Dwek (2001). 12
2.6 This figure shows different EBL model, adapted from Dwek & Krennrich (2013). 13
2.7 Schematic representation of the Bremsstrahlung interaction. . . 15
2.8 Schematic illustration of the inverse Compton scattering proses. 15
2.9 An illustration of nuclear transitions decay. 16
2.10 An illustration of the electric-positron annihilation. 16
2.11 The Photoelectric Effect. 18
2.12 Compton Scattering. 18
2.13 The Pair Production Effect. 19
2.14 Electromagnetic Cascades. 19

3.1 The lifetime of the star on the main sequence 24
3.2 The initial mass function 25
3.3 The star formation rate 26
3.4 The EBL energy density obtained using Razzaque *et al.* (2009). 27
3.5 The EBL energy density obtained uses the Finke *et al.* (2010) approach. 28
3.6 Mean SFR derived from the Guo et al. 2013 galaxy catalogue. . 30
3.7 SQL query to retrieve stellar mass, SFR and position. 31
3.8 The SFR radial profile at redshift (0.0). 32

4.1 The fluctuations in the SFR density. 35
4.2 Six overlapping trumpets at different redshifts. 35
4.3 The EBL energy density for Model B described in section 3.1 for different redshifts. 37

4.4 Gamma-ray opacity of the Universe at different redshifts, with energy range of 0.1 to 1 TeV. 38
4.5 The difference between the γ-ray opacity and its upper and lower limits in percentage. 39

List of Tables

3.1 Parameters of IMF models 24
3.2 Parameters of SFR models 26
3.3 Dust parameters from Finke *et al.* (2010). 29

List of Physical Constants and Symbols

Symbol	Name	Value	Unit
Ω_m	Matter Density	0.3	
Ω_Λ	vacuum Energy Density	0.7	
h_0	Dimension-Less Hubble Parameter	0.7	
H_0	Hubble Constant	100	km s^{-1}Mpc^{-1}
h	Planck's Constant	6.626196×10^{27}	erg s
$\hbar$	Rationalized Planck's Constant	1.0545919×10^{27}	erg s
c	Speed of Light in Vacuum	$2.997924562 \times 10^{10}$	cm sec^{-1}
e	Elementary Charge of an Electron	-1.602×10^{-12}	esu
m_e	Rest Mass of the Electron	$9.1093897 \times 10^{-28}$	g
k	Boltzmanns Constant	1.3806×10^{-16}	erg K^{-1}
$M_\odot$	Solar Mass	1.99×10^{33}	g
$T_\odot$	Solar Temperature	5777	K
$R_\odot$	Solar Radius	6.955×10^{10}	cm
$L_\odot$	Solar Luminosity	3.846×10^{33}	erg s^{-1}
$t_\odot$	Solar Lifetime	11	Gyr
eV	Electron Volt	$1.6021772 \times 10^{-12}$	erg
ϵ	Extragalactic Background Light Energy		erg
$t_\star$	Main-Sequence Lifetime of a Star		Gyr
$\mathcal{L}_\nu$	Spectral Luminosity Density		erg cm^{-1}
I_ν	Spectral Intensity		
r_0	Classical electron radius	$2.8179403267 \times 10^{-13}$	cm
$\xi(M)$	Initial Mass Function		
μG	Micro Gauss	10^{-6}	Gauss

List of Abbreviations

Abbreviation	**Meaning**	**Page**
AGN	**A**ctive **G**alactic **N**uclei	2
BE	**B**ackward **E**volution	9
CCE	**C**osmic **C**hemical **E**volution	9
CMB	**C**osmic **M**icrowave **B**ackground	2
CSFR	**C**osmic **S**tar-**F**ormation **R**ate	8
EBL	**E**xtragalactic **B**ackground **L**ight	2
FE	**F**orward **E**volution	9
FRD10	**F**inke **R**azzaque **D**ermer 20**10**	27
UV	**U**ltra**v**iolet	2
ISM	**I**nter**s**tellar **M**edium	6
IGM	**In**ter**g**alactic **M**edium	7
PAH	**P**olycyclic **A**romatic **H**ydrocarbons	7
FIRAS	**F**ar **I**nfrared **A**bsolute **S**pectrophotometer	8
VHE	**V**ery **H**igh **E**nergy	8
IR	**I**nfer**r**ed	2
IMF	**I**nitial **M**ass **F**unction	6
LF	**L**uminosity **F**unction	10
RDF09	**R**azzaque **D**ermer **F**inke 20**09**	22
SAM	**S**emi-**A**nalytical **E**volution	5
SED	**S**pectral **E**nergy **D**istribution	6
SFR	**S**tar **F**ormation **R**ate	9
ΛCDM	Λ **C**old **D**ark **M**atter	1
WMAP5	**Five-Year W**ilkinson **M**icrowave **A**nisotropy **P**robe	13
COBE	**Co**smic **B**ackground **E**xplorer	9
DIRBE	**D**iffuse **I**nfrared **B**ackground **E**xperiment	8
SPL	**S**ingle **P**ower **L**aw	23
BPL	**B**roken **P**ower **L**aw	23
SQL	**S**tructured **Q**uery **L**anguage	30
SDSS	**S**loan **D**igital **S**ky **S**urvey	29
6DF	6-**D**egree **F**ield survey	29
2MASS	**T**wo **M**icron **A**ll-**S**ky **S**urvey	29

1 Introduction

1.1 Background

In 1823 Heinrich Olbers argued that the night sky should be very bright if the universe were static, homogeneous and infinite in size which was back then a reasonable assumption. Olbers' argument was as follows: consider (cosmic) spherical shells of different radii R, and of identical thickness t. The volume of the shells is proportional to R^2, so the number of stars or galaxies within the shells is also proportional to R^2 (Bernstein, 2000). On the other hand, the amount of light from an object at distance R is proportional to $1/R^2$. Consequently, every shell contributes the same amount of light. Since the universe is assumed to be infinite and homogeneous, the constant contributions of the infinite number of shells add up to an infinite brightness of the sky during both day and night. The night sky should therefore not be dark.

This contradiction is commonly known as Olbers' paradox. Olbers' paradox challenges the conjecture that the Universe is static, infinite and homogeneous (Bernstein, 2000). Olbers' paradox may be resolved by more recent cosmological discoveries. Edwin Hubble's discovery that the Universe is expanding has displaced the idea that the Universe is static. According to Hubble's Redshift-Distance Law the light from the distant sources is strongly red-shifted. Therefore, the light from distant galaxies maybe shifted out of the visible range. This provides a partial solution to Olbers' paradox, which is the possible attenuation of distant sources in the optical bands. However, it implies that the Universe should be bright in other regions of the electromagnetic spectrum. The Big-Bang theory finally provided a satisfactory solution for Olbers' paradox. The idea that the Universe possesses a finite age implies that photons from very distant sources have not had sufficient time to reach Earth. According to the currently most accepted cosmological paradigm we are living in a Lambda Cold Dark Matter (ΛCDM) Universe, which started with the Big-Bang some 14 Billion years ago.

In fact the night sky is not completely dark. Several sources of light brighten it. Among these is a diffuse source of light called the Extragalactic Background Light (EBL). The light it contributes to the sky brightness is in the Ultraviolet (UV) to Infrared (IR) range, and maks up less than 1% (Bernstein, 2000). Measurements of the diffuse Extragalactic Background Light (EBL) have been difficult because of dominant foregrounds of galactic, zodiacal and terrestrial sources, which also cause systematic bias against detection of faint or low surface brightness of individual galaxies and intergalactic stars. However, measurements of the diffuse EBL do not suffer from the surface brightness selection effects. Thus, the EBL can provide a useful integral constraint on star formation models and the baryonic matter content of the Universe (Bernstein, 2000).

EBL is defined as the accumulated light released from the time of decoupling after the Big-Bang until now by all extragalactic sources, resolved and unresolved, at wavelengths between $0.1\,\mu$m upto $1000\,\mu$m. The EBL contains a great deal of information regarding the evolution and the structure of the Universe and its astrophysical components. This makes it a topic of great interest.

Note that the EBL includes neither the Cosmic Microwave Background (CMB) radiation nor foreground radiation from the Milky Way (Yuan *et al.* , 2012; Hauser & Dwek, 2001; Dwek & Krennrich, 2013). X-rays and γ-rays are not considered to be part of the EBL even though they are produced by extragalactic sources. This is because they are generated by difference production mechanisms. X-rays and γ-rays are produced by accretion-power in Active Galactic Nuclei (AGN), whereas the EBL is the accumulated radiation emitted by the stellar component of galaxies.

From the discussion above, it is clear that measuring the EBL is a powerful tool for understanding the star formation history of the Universe. However, there are considerable difficulties in measuring the EBL directly. For example, separating it from the zodiacal light of our solar system or from the foreground light of our Galaxy poses serious challenges (Costamante, 2013). Indirect measurement of the EBL can be achieved by observing the attenuation of γ-ray spectra from distant objects such as Quasars [1]. Gamma-rays traveling through the Universe interact with EBL photons to produce electron-positron (e^-, e^+) pairs. This interaction provides an efficient absorption mechanism for high energy γ-rays. The amount of EBL in the line of sight from the sources to the observer can be inferred by comparing observed quasar spectra with models of spectra that neglect absorption (Yuan *et al.* , 2012).

The EBL is also related to radio, and supernova neutrino backgrounds. The correlation between radio emission and IR radiation from star forming galaxies has been well established in several papers (e.g., Lisenfeld *et al.* 1996; Condon *et al.* 1991). These results can be used to estimate the contribution to the background radio emission from star forming galaxies (Dwek & Barker, 2002; Haarsma & Partridge, 1998; Ponente *et al.* , 2011). Supernova rate and the resulting neutrino flux can be estimated using the total EBL intensity, which is mostly powered by massive stars that eventually burn out and end their lives in a supernova explosion.

[1] Quasar: are extremely luminous galaxies powered by AGN (Costamante, 2013; Ackermann *et al.* , 2012)

Conversely, one can also use the total intensity of the EBL to the supernova rate and their neutrino fluxes (Horiuchi *et al.* , 2009; Beacom, 2010) to determine the supernova contribution to the background radio emission. In addition to the IR emission, stars with high mass also emit in radio through free-free emission mechanism during their evolution in the main sequence, and through synchrotron emission mechanism during the supernova remnant phase.

Most of the background X-rays produced by the AGNs are absorbed by surrounding dust (Mushotzky *et al.* , 2000), and re-emitted in the mid-IR range (Franceschini *et al.* , 2002). This can be used to estimate the EBL density in certain energy ranges. Soifer *et al.* (2008) and Treister *et al.* (2006) have shown that, at $24\,\mu$m, 15% of the EBL intensity can be degraded from AGNs.

Interaction between high energy γ-rays emitted from Blazars (AGN's with a relativistic jet directed to Earth), and the EBL through photon-photon interaction can be used to set limits on both spectra at the ranges of energy where these interactions occur (Dwek & Krennrich, 2013).

1.2 Problem Statement

Several models have been proposed to predict the evolution of EBL with time/redshift (Finke *et al.* , 2010; Razzaque *et al.* , 2009; Gilmore *et al.* , 2012). Also, astronomers have tried to observe and model the signature of the EBL density on the spectrum of distant γ-ray sources (Yuan *et al.* , 2012; Hauser & Dwek, 2001; Ackermann *et al.* , 2012). These observations show that there are fluctuations in the EBL density (Kashlinsky *et al.* , 1996b,a; Vogeley, 1997). However, to the best of our knowledge, none of the available models consider the EBL fluctuations and their impact on the spectrum of the distant sources.

1.3 Aims

The aim of this work is to model the EBL and, in particular, the impact of its fluctuations. To achieve this we use theoretical models to study the distribution of EBL in the Universe and explore both small and large fluctuations in the EBL. Finally we investigate the correlation between these fluctuations and the γ-ray opacity of distant sources.

1.4 Outline

The material of this thesis is set as follows. A brief introduction to the EBL research has been presented in this chapter. Chapter 2 is devoted to a literature review. Methods for modelling the EBL are described in Chapter 3. Chapter 4 presents our results. Conclusions that can be drawn from our results are discussed in Chapter 5.

2
Literature Review

This chapter is in two parts. In the first, we defined EBL and outline some of its properties. In the second we discuss some properties of γ-ray radiation that are important to the later chapters of this thesis. In detail, EBL is defined in section 2.1.1. Sources of EBL are discussed in section 2.1.2. The measurement of the EBL is provided in section 2.1.3, followed by the EBL density and models in sections 2.1.4 and 2.1.5, respectively.

The γ-ray emission mechanisms and sources are discussed in sections 2.2.1 and 2.2.2 respectively. Sections 2.2.3 and 2.2.4 disccus the interaction of γ-ray with matter and electro- magnetic spectrum respectively. Finally, γ-ray detection is presented in section 2.2.5.

2.1 Extragalacitc Background Light

2.1.1 Definition of the EBL

Extragalactic Background Light is defined as the accumulated light released from the time of the decoupling era after the Big Bang until the present time. In other words, EBL is the light integrated from unresolved and resolved extragalactic sources. Because the CMB comes from a different source, the CMB light is not considered to be part of the EBL spectrum. The EBL energy density is the second most dominant energy density following the CMB density (Dwek & Krennrich, 2013). This definition of the EBL excludes the low energy foreground radiation from the Milly Way and the solar system as well as the high energy background radiations such as X-rays and γ-rays. The latter are not considered to be part of the EBL because they are produced by different emission mechanisms.

Figure 2.1 shows a static snapshot of the EBL spectrum model at redshift $z = 0$ (Primack *et al.* , 2005). The EBL spectrum is distributed between 0.1 up to 1000 μm $\sim$ (10^{-3} up to 10 eV). It has two humps: a first hump around the short wavelengths

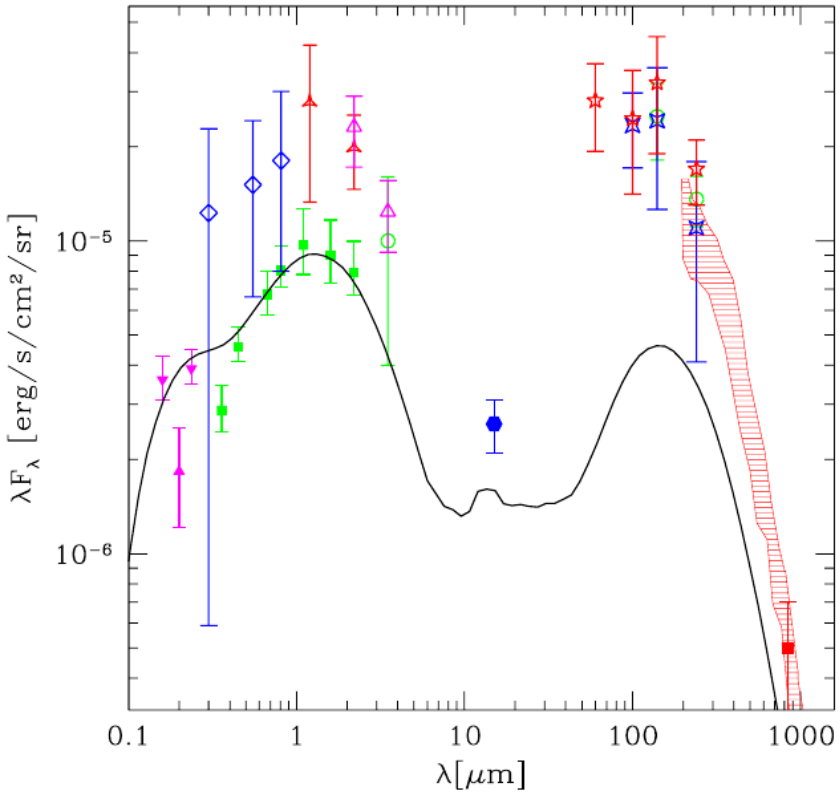

Figure 2.1: The predicted EBL spectrum displayed as black line compared with observations, from Primack *et al.* (2005). The filled squares are from the Hubble Deep Field, filled hexagons are taken from Elbaz *et al.* (2002), the shaded red region is adapted from FIRAS and the 140 μm and 240 μm points are from DIRBE.

from 0.1 μm up to 10 μm, and a second between the 10 μm and 1000 μm. The proposed reasons for these humps will be discussed in more detail in section 2.1.2. The evolution of the EBL with redshift can be computed, for example, with the help of Semi Analytic Galaxy Evolution Models (SAM), as proposed by Primack *et al.* (2005). Figure 2.2 (Primack *et al.* , 2005) shows the intensity variation of the EBL as a function of wavelength and redshift.

2.1.2 Contributors of the EBL

In section 2.1.1, we noted that the EBL spectrum has two humps. The first hump is attributed to contributions from different types of stars (see section 2.1.2.1). Because of the expansion of the universe the light of distant stars / galaxies is redshifted. The light which has been absorbed by the interstellar medium (dust and gas) within the galaxies and remitted at longer wavelengths is responsible for the second hump in the EBL spectrum detailed in section 2.1.2.2. One can further differentiate the contribution from AGNs which will be detailed in section 2.1.2.3.

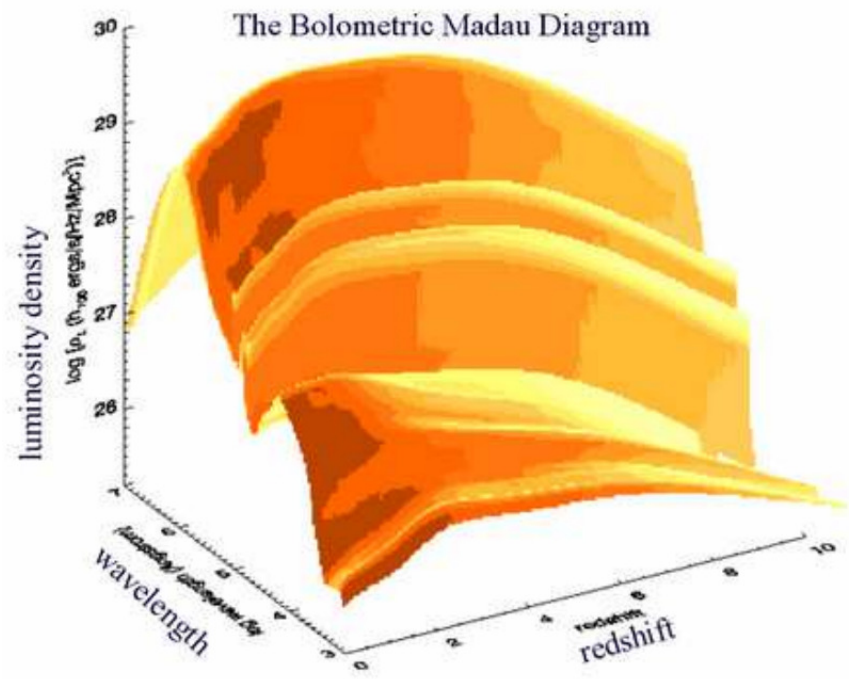

Figure 2.2: The evolution of the EBL luminosity as a function of wavelength with redshift proposed by Primack *et al.* (2005).

2.1.2.1 Stellar Contribution

The UV to IR spectrum of the EBL is dominated by stellar emission with different metallicity at all redshifts since the formation of the first stars. Colour and spectral analysis of distant quasars suggests the presence of heavy elements [1] (metals) in the early universe. According to current star formation models, the first stars, called Population III (PopIII), with little or no heavy elements exhausted their fuel quickly and hence produced the first heavier elements as they went supernovae, thereby metal enriching the Interstellar Medium (ISM). Once the star forming cloud reaches a critical metallicity, PopIII stars are not formed any longer (see e.g., Prialnik 2000; Omukai *et al.* 2005; Schneider 2006). They are replaced by Population II stars (PopII) with lower masses and "Salpeter-like" Initial Mass Functions (IMF) (e.g. Schneider 2006). Population II and Population III (though PopIII are not observationally confirmed yet) are believed to contribute to the formation of the young and metal-rich Population I stars (Prialnik, 2000).

A common feature of actively star forming galaxies are starburst regions where brief episodes of star formation take place. The distribution of the stellar masses formed in the same starburst episode is described by global IMF. The lifespan and cumulative emission of a star is mainly determined by its mass and metallicity. Therefore, massive stars ($M > 8\,M_{\odot}$) fuse hydrogen into helium rapidly leading to a very short life span ($\sim 10^7$ yrs). In contrast, low mass stars go through a slow emission process; hence their longer life span. While massive stars emit the majority of their energy at UV wavelengths, low mass stars emit mainly at optical wavelength and follow the main sequence. The Spectral Energy Distribution (SED) of individual

[1] heavy elements mean the metals with atomic number ($Z > 2$)

starbursts, which depends on the starburst age, must be integrated over the entire stellar population of a given galaxy.

The spectral energy distribution of a galaxy is affected by the absorption and reradiaiton of starlight by dust and Hydrogen in the ISM. In the far-UV, Lyman continuum absorption by hydrogen in the Intergalactic Medium (IGM) limits the emission from the stars above 13.6 eV, which is the ionizing energy for neutral Hydrogen (HI). Moreover, radiation below 13.6 eV can excite the Hydrogen in the IGM. The absorbed energy can then be remitted again in the UV, visible and IR, due to the recombination of free electron with the Hydrogen ions, or due to dexcitation of the Hydrogen atom.

2.1.2.2 Dust Contribution

The dust in the ISM is composed mainly of grains made of graphite and silicate with various sizes ranging from 10^{-9} to 10^{-5} m and Polycyclic Aromatic Hydrocarbons (PAH; Dwek 2001). The origin of the Infrared part of the EBL spectrum ($10-1000$ μm) is assumed to be the dust in the ISM, since ISM is made of dust grains from the universal dust factory around giant stars due to their mass loss. This dust is powered by the hot elements in the ISM and remit its energy in the longer wavelengths IR. The contribution of the dust to the final SED of the EBL depends on many factors. For instance, grain size and its abundance, the optical properties of the dust, lumpiness of the ISM and distribution of the dust compared with the radiation sources in the galaxies (Dwek, 2001).

Observations show that a small amount of dust can significantly increase a galaxy's brightness in the mid-IR to far-IR range. The brightness in the mid-IR to far-IR range exceeds that in the optical and near-IR range (Kashlinsky, 2005). Furthermore, with the right environment, re-radiation from the dust can be the dominant emission in starburst regions (Kashlinsky, 2005). The presence of dust around a black hole in the center of a galaxy absorbs a significant amount of the AGN radiation which then is re-emitted in the far-IR regime (Dwek, 2001).

2.1.2.3 AGN Contribution

The contribution from the AGNs to the total EBL density is relatively small compared with the stellar contribution (e.g., Malkan & Stecker 1998; Lagache & Puget 2000; Elbaz *et al.* 2002). The maximum contribution of a black hole via accretion processes to the total EBL density observed today is less than 20% of the total EBL, and can be calculated as $\left(\frac{c}{4\pi}\epsilon\rho_{BH}c^2\left\langle(1+z)^{-1}\right\rangle\right)$, where $\rho_{BH} = (3\pm2)\times10^6$ h$M_\odot$Mpc^{-3} is the estimated mean mass density of black holes in the Universe, c is the speed of light, $\epsilon \sim 0.7$ is the conversion efficiency factor from rest mass into radiated energy and the mean redshift distribution of AGNs is at $\langle z\rangle \sim 2$ (Madau & Pozzetti, 2000).

2.1.3 Measurements of the EBL

Direct measurements of the EBL have been difficult because of dominant foregrounds of galactic and zodiacal light from which it has to be separated (see Hauser & Dwek

2001 for a review). Because of these difficulties direct measurements provide only lower and upper limits on EBL intensity.

A solid lower limit on the EBL can be derived from the integrated light coming from resolved galaxies (e.g., Madau & Pozzetti 2000; Fazio *et al.* 2004; Béthermin *et al.* 2010). This approach, however, is less reliable at longer wavelengths since unresolved galaxies become a source of confusion, limiting the sensitivity of detectors. These limitations can be partially avoided by extrapolation of the differential source counts via improved data analysis techniques (i.e., stacking analysis Dole *et al.* 2006).

Several lower and upper limits have been placed in the IR wavelength region with the aid of ground- and space-based observations and stacking analysis. For instance, the Diffuse Infrared Background Experiment (DIRBE; Hauser *et al.* 1998) at 140 μm, and the Far-IR Absolute Spectrophotometer (FIRAS) detections (Fixsen *et al.* , 1998) at longer wavelengths (see Dwek & Krennrich 2013 for a summary of recent observation). However, the EBL is poorly constrained in the wavelength region $\approx 10 - 70\,\mu$m, where the thermal emission from interplanetary dust (zodiacal light) is dominant (Kelsall *et al.* , 1998). On the other hand, the fact that high energy gamma-ray photons can pair produce with low energy photons in the EBL provides an indirect but effective method to measure the EBL. The EBL intensity in the optical-IR regions can be constrained by means of measured spectra of Very High Energy (VHE) γ-ray sources (Dwek & Krennrich, 2013).

2.1.4 EBL Density

The total EBL intensity I_{EBL} can be expressed as the integral of the comoving luminosity density $\mathcal{L}$ over redshift z:

$$I_{EBL} = \left(\frac{c}{4\pi}\right) \int_0^\infty \mathcal{L}(z) \left|\frac{dt}{dz}\right| \frac{dz}{1+z}, \tag{2.1}$$

where $\mathcal{L}(z)$ is the luminosity density in the comoving volume emitted for all objects at the rest frame and $\left|\frac{dt}{dz}\right|$ is the cosmic time redshift relationship, and it is given by:

$$\left|\frac{dt}{dz}\right| = \left(H_0(1+z)[(1+z)^2(1+\Omega_M z) - z(2+z)\Omega_\Lambda]^{1/2}\right)^{-1}, \tag{2.2}$$

where H_0, Ω_M and Ω_Λ are the Hubble parameter, the normalized matter density and the normalized dark matter density respectively.

The main contribution to the comoving luminosity density comes from starlight integrated over cosmic time. Although AGN emission can dominate the optical/IR output of an individual galaxy, on a global scale the contribution to the total IR background is much smaller. Infrared observations show that AGNs produce a small fraction, between 13 % and 19 %, of the mid-IR spectrum (Hainline *et al.* , 2009). Consequently, the total comoving luminosity density can be used as a direct measure of the Cosmic Star Formation Rate (CSFR) at a given redshift, which in turn makes the EBL an integral measure of cosmic star-formation history. Around 10 to 20 % comes from mass accretion processes onto a central black hole (Madau & Pozzetti,

2000).

Using the dependence of Star Formation Rates (SFRs) on star-formation history of a given star-forming galaxy as well as the relation between a bolometric luminosity and SFR (Ψ) on Salpeter stellar IMF, Dwek *et al.* (2011) converted CSFR to a bolometric luminosity ($L_{bol} = 7.5 \times 10^9 \Psi\ M_{\odot}\mathrm{yr}^{-1}$ for a starburst age of 100 Myr). This integrated intensity of the CSFR is then limited by:

$$I_{EBL} = 21 - 66 \text{ nW m}^2\text{sr}^{-1} \tag{2.3}$$

See Dwek & Krennrich (2013) for a summary of the current limits on the EBL.

2.1.4.1 Fluctuation Measurements and EBL Density

The EBL density in the Universe is generated from discrete galaxies and other primordial stellar sources, therefore, the fluctuation in the spatial distribution of these sources leads to fluctuations in the intensity of the EBL (Dwek & Krennrich, 2013). Several studies have been carried out to investigate these fluctuations. For instance, Shectman (1973, 1974) investigated the anisotropy in the optical regime, where Kashlinsky *et al.* (1996c) investigated clustering in the near-IR region using Cosmic Background Explorer (COBE) and DIRBE Maps. Although one cannot determine the EBL density by only knowing the fluctuations in the EBL (Dwek & Krennrich, 2013), the fluctuation measurements can be used to derive a limit on the EBL density at certain regions of the spectrum (Pénin *et al.* , 2012). Furniss *et al.* (2015) found a correlation between VHE-emitting sources and cosmic voids along the line of sight. They have also estimated less than 10% attenuation of γ-ray decrease for highly attenuated VHE sources.

2.1.5 Models of the EBL

In order to predict the SED of the EBL various factors have to be taken into account, including the stellar IMF, CSFR, metallicity evolution, the amount of energy emitted by AGNs, and nuclear and gravitational processes (Hauser & Dwek, 2001). Furthermore, in a dusty universe, though the total EBL intensity remains unchanged, the energy is redistributed by absorption and re-emission processes over the entire spectrum (Hauser & Dwek, 2001). However, constructing the re-emitted part of the EBL spectrum has proven to be challenging since it depends on several factors, such as the dust composition, size distribution, abundance and their evolution over time. Furthermore, the spatial distribution of dust relative to the radiative sources has an impact on the re-emission process (Dwek & Krennrich, 2013).

Several models have been developed to derive an overall spectrum of the local EBL and its evolution based on the knowledge of galaxy evolution and SFR incorporated with observational constraints. The models use different strategies to determine the evolution of the comoving luminosity density, $\mathcal{L}(z)$, as a function of redshift which may be categorised in four groups. A brief description will be given for each category, in the following sections. The Backward Evolution model (BE) is described in section 2.1.5.1 and the Forward Evolution model (FE) is given in section 2.1.5.2. The Cosmic Chemical Evolution models (CCE) are discussed in section 2.1.5.3, while the Semi-analytical Models (SAM) are reviewed in section 2.1.5.4.

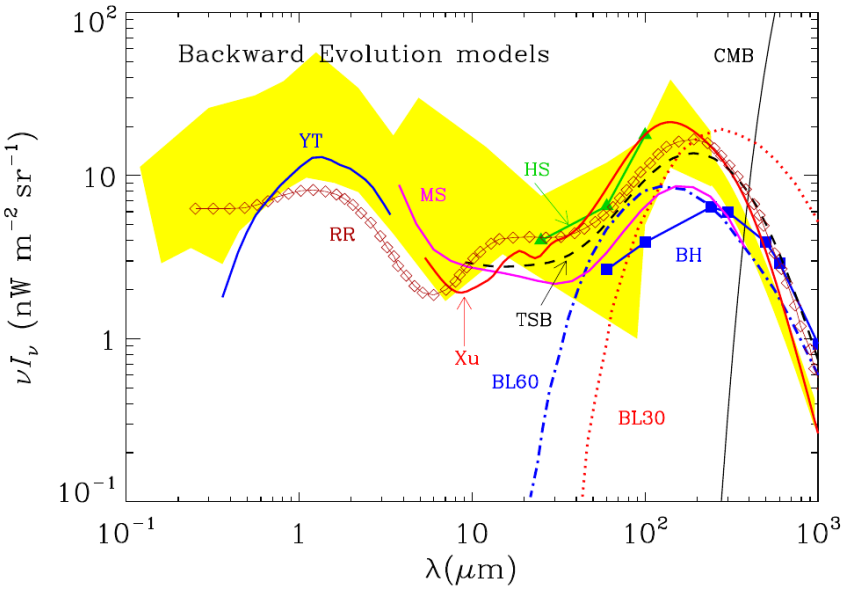

Figure 2.3: Different BE models predicting the EBL spectrum. The solid squares represent the prediction of the (BH) model by Beichman & Helou (1991); solid triangles is the (HS) model (Hacking & Soifer, 1991); the purple line is the (MS) (Malkan & Stecker, 1998); the red dotted line and the blue dash-dot line are the (BL30) and (BL60) models respectively (Blain & Longair, 1993). The solid red line is the (Xu) model by Xu (2000); black dashed line is (TSB) model (Tan *et al.* , 1999); open diamonds is the (RR) model by (Rowan-Robinson, 2001) and the blue solid line is the (YT) by (Yoshii & Takahara, 1988). The yellow shaded area are the limits from observation. The figure is adapted from Hauser & Dwek (2001).

2.1.5.1 Backward Evolution Models (BE)

This method determines the local $\mathcal{L}(z)$ at $z = 0$ using low-red shift observations of galaxy Luminosity Functions (LFs) and extrapolates them to higher redshifts (e.g., Malkan & Stecker 1998, 2001; Rowan-Robinson 2001; Stecker *et al.* 2006). In this model, the SED of galaxies, constructed from existing galaxy populations in the local Universe, is extrapolated backwards in time. The luminosity density is then given by the convolution of the LF with the integrated SED of different types of galaxies.

Evolution of the LF can be determined either directly from observations of sources with known redshift and complete number counts (e.g., Dunne *et al.* 2000; Rodighiero *et al.* 2010) or by assuming a functional form for the LF redshift evolution (e.g., Rowan-Robinson 2001; Stecker *et al.* 2006). Evolution to the LF can also be introduced by changing the relative number counts of different galaxy types with redshift (e.g., Lagache *et al.* 2003; Rowan-Robinson 2001, 2009; Domínguez *et al.* 2011). More recently, Helgason & Kashlinsky (2012) constructed a relatively robust BE model using evolving galaxy number count at UV to mid-IR wavelengths. Figure 2.3 shows different models using the BE approach (adapted from Hauser & Dwek 2001).

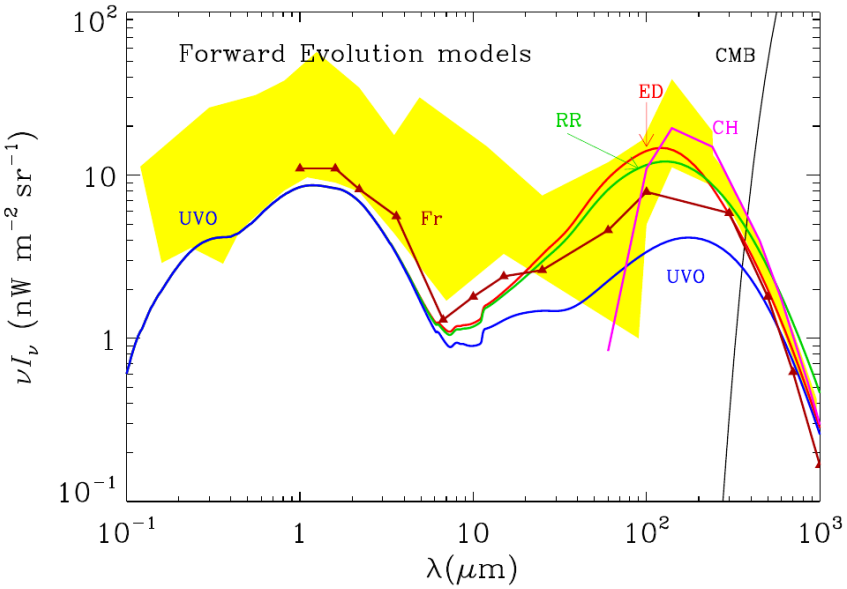

Figure 2.4: Comparison between predictions of different FE models and the observed EBL spectrum. Where the solid triangles is (Fr) model by (Franceschini *et al.* , 1994); solid violet line is (CH) model by (Calzetti & Heckman, 1999); red, green, blue solid lines are the (ED), (RR), (UVO) models respectively by (Dwek, 1998). The shade yellow area is the limits from observation. This figure is adapted from Hauser & Dwek (2001).

On of the advantages of the BE models is that they allow for a straight forward comparison between the predicted galaxy properties such as color-magnitude, number-magnitude and number-redshift, and the observed properties. This model is a purely phenomenological, and it has no physical processes involved in constraining the EBL intesity, such as star formation or radiative transfer processes that take place in the galaxy evolution (Dwek & Krennrich, 2013).

2.1.5.2 Forward Evolution Models (FE)

This approach begins with primordial initial conditions for star-formation and follows galaxy evolution forward in time, whereby it is ensured that the initial conditions are in agreement with observations (e.g., Dwek *et al.* 1998; Razzaque *et al.* 2009; Finke *et al.* 2010). These models use the redshift dependence of CSFR over which the SED of stellar populations are integrated to determine $\mathcal{L}_\nu(\lambda, z)$ as a function redshift.

The determination of the CSFR entails uncertainties due to the effect of dust on the scattering, absorption of UV-optical starlight, and thermal reradiation at IR wavelength. Furthermore, the conversion of CSFR to total bolometric luminosity depends on our knowledge of the stellar IMF, which is a poorly determined parameter at high redshift. Once the CSFR is obtained, it is used to convolve models for the SED of stellar population (e.g., Fioc & Rocca-Volmerange 1997; Leitherer *et al.* 1999; Bruzual & Charlot 2003; Maraston & Strömbäck 2011) to determine the evolving stellar bolometric and spectral luminosity density as function of redshift.

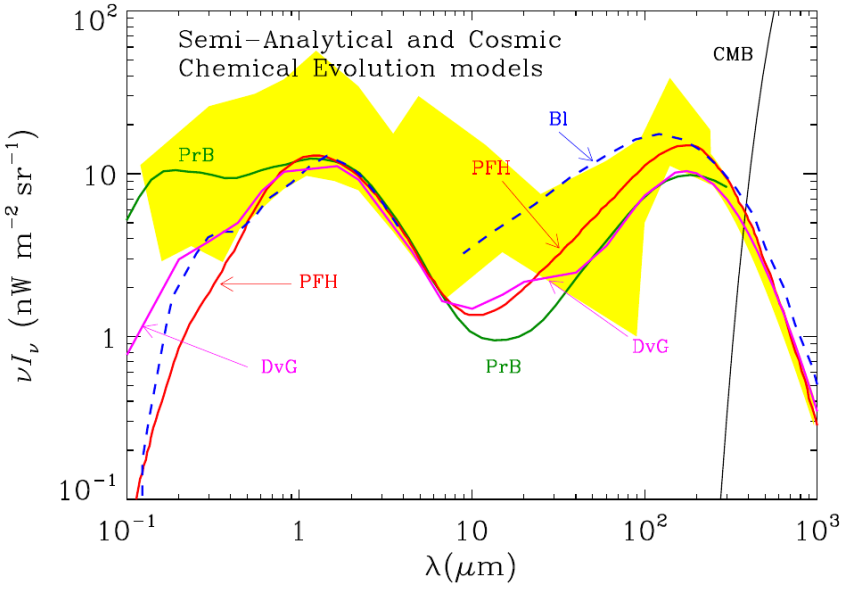

Figure 2.5: Comparison between the predictions of different CCM and SAM models and the observed EBL spectrum. The SAM models: the green line is (PrB) model by (Primack *et al.* , 1999); the violet line is (DvG) model by (Devriendt & Guiderdoni, 2000) and the blue line is (Bl) model by (Blain *et al.* , 1999). The CCE models: the red line is (PFH) model by (Pei *et al.* , 1999). The shade yellow area is the limits from observation. This figure is adapted from Hauser & Dwek (2001).

Figure 2.4 shows different models using the FE approach (adapted from Hauser & Dwek 2001).

To determine the SED of a galaxy one can use radiative transfer models (e.g., Silva *et al.* 1998; Gordon *et al.* 2001; Nenkova *et al.* 2000), or use observational approaches to obtain the fraction of UV-optical light absorbed by dust, and the re-radiated IR spectrum statistically. The combination of population synthesis models with radiative transfer models provides a useful tool to obtain the UV to radio SED of a given galaxy. This makes FE models successful in reproducing the SED of individual galaxies, and the global characteristics of the EBL. However, such models do not allow one to take into account galaxy interactions and associated changes in star formation rate, or morphological evolution of galaxies.

2.1.5.3 Cosmic Chemical Evolution Models (CCM)

This is a modeling approach which deals with globally averaged properties of the universe. These models only consider basic galaxy ingredients, i.e., interstellar gas, metallicity, and radiation. In this model, chemical evolution equations, that are similar to those used for chemical evolution of the Milky Way (e.g., Audouze & Tinsley 1976; Tinsley 1981; Pagel 2001), are used to follow the evolution of the average stellar, gaseous and radiation content in comoving volume elements in a self-consistent manner (Hauser & Dwek, 2001).

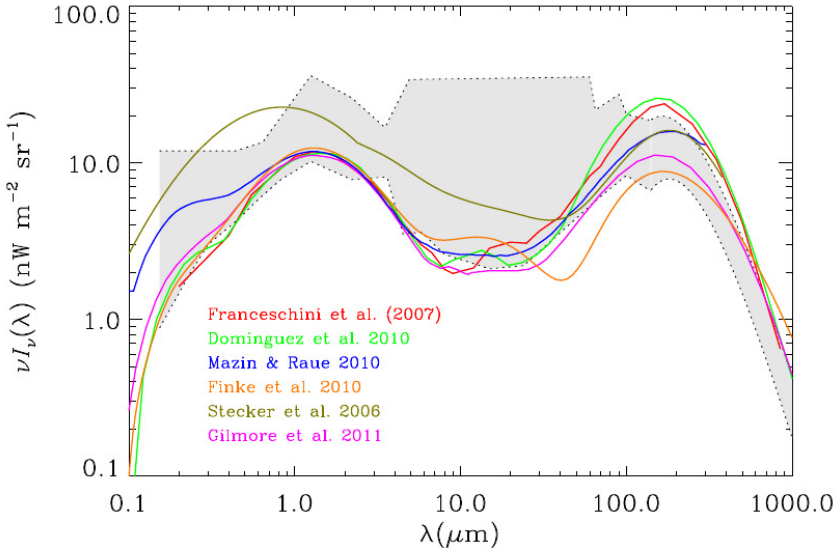

Figure 2.6: The different EBL model adapted from Dwek & Krennrich (2013). The BE are (Stecker *et al.* , 2006) in yellow line, (Franceschini *et al.* , 2008) in red line and (Domínguez *et al.* , 2011) in green line. The FM (Finke *et al.* , 2010) in orange line. The SA (Gilmore *et al.* , 2012) in purple line. (Mazin & Raue, 2007) in blue line. The shaded gray area is the EBL limit determined by the intensity of IGM for the lower limits and by the absolute measurements of the EBL for the upper limits.

2.1.5.4 Semi-analytical Models (SAM)

This model applies physically motivated descriptions for the physical processes that determine formation and evolution of galaxies in a ΛCDM Universe using initial conditions derived from observations such as the Five-Year Wilkinson Microwave Anisotropy Probe (WMAP5) observations. These models follow the growth and merger history of dark matter halos, and the development of galaxies formed as baryonic matter fall into the potential wells of these halos, and the physical evolution of its baryonic component. SA models, therefore, account for factors determining the fate of gas in-fall into dark matter halos. These include, the effect of gas cooling, star formation in a multiphase ISM, AGN and supernova feedback, chemical enrichment of the ISM, material exchange with the IGM through in-fall and Galactic winds, galaxy merger, etc. (e.g., Kauffmann *et al.* 1993; Cole *et al.* 1994; Somerville & Primack 1999). Figure 2.5 shows different models using the SAM with CCM approaches (adapted from Hauser & Dwek 2001). Similar to other EBL models, reproducing galaxies SED is complicated by extinction effects. The correct determination of the amount of starlight absorbed by dust and re-emitted is crucial. In addition, SA models are complex and computationally quite expensive. They depend on the modelling of several physical processes, some poorly understood, to derive galaxy properties. Despite these difficulties, SA models managed to successfully reproduce various observed properties of galaxies (e.g., references mentioned above plus Fontanot *et al.* 2009; Fontanot & Somerville 2011; Younger & Hopkins 2011). Therefore they provide a good base for the computation of the EBL, which is simply the integrated light of all the modelled galaxies.

2.2 Gamma-ray Astrophysics

Photons with high energies, above a few hundred keV, are classified as γ-rays. The high energy of γ-rays can only be produced by powerful processes in the Universe. In section 2.2.1 we will discuss various proposed mechanisms of γ-ray emission. Astronomical sources will be described briefly in section 2.2.2. In sections 2.2.3 and 2.2.4 we describe the interaction of γ-rays with matter and electromagnetic radiation, respectively. The detection methods of γ-rays are discussed in section 2.2.5, and finally its attenuation by EBL is reviewed in section 2.2.5.

2.2.1 Gamma-ray Emission Mechanisms

Two processes are known to produce γ-rays: thermal and non-thermal emission processes. Thermal emission can be modeled as a black body, for instance according to Wien law, a 10 Mev γ-rays need temperature of order 10^{10} K to be emitted, however such temperature is not available in our Universe. Nevertheless, non-thermal processes which involve interaction between charged particles and electric or magnetic fields can produce very high energy γ-rays.

Synchrotron and Bremsstrahlung Radiation

One of the well studied phenomena in electrodynamic is that of the production of electromagnetic radiation by accelerating charged particles in magnetic or electric fields (Jackson, 1998). The mass, momentum and charge of the accelerated particle, in addition to the orientation and strength of the field, are the main parameters that affect the spectral energy, the angular distributions and the amount of emitted radiation.

Synchrotron radiation is a free-free emission, which takes place when a charged particle is accelerated by an electric or a magnetic field. The energy of the emitted photon due to the interaction between a high energy electron (cosmic ray) with energy (E_e) and an interstellar magnetic field (B) where μG=10^{-6} Gauss, is given by equation 2.4.

$$E_\gamma \simeq 0.05 \cdot \left(\frac{E_e}{(\mathrm{TeV})}\right)^2 \cdot \frac{B}{3\mu G}(\mathrm{eV}), \tag{2.4}$$

The strong magnetic fields of order 10^{10} G associated with pulsars or the surface of neutron stars are sufficient for producing gamma photons (e.g., Ruderman & Sutherland 1975; Schönfelder 2001).

Bremsstrahlung (braking radiation) is also a free-free emission, occurring when charged particles are decelerated by an external electric field or when passing through matter. Figure 2.7 shows a sketch of the process as an electron passes near to the nucleus of an atom its direction gets deflected in other words it is losing kinetic energy and hence a photon is emitted. The energy of the emitted photon E_γ is given in equation 2.5,

$$E_\gamma = (\gamma - 1)m_e c^2, \tag{2.5}$$

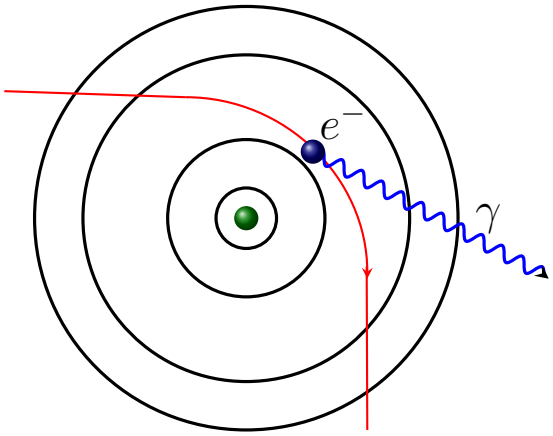

Figure 2.7: Schematic representation of the Bremsstrahlung interaction.

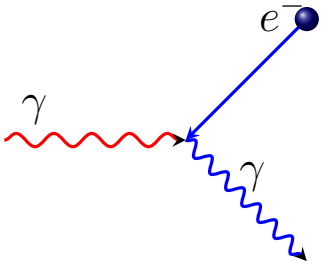

Figure 2.8: Schematic illustration of the inverse Compton scattering proses.

where $\gamma = \left(\sqrt{1-\frac{v^2}{c^2}}\right)^{-1}$ is the Lorentz factor. The spectrum of the braking radiation is characterized by its flatness and sharp drop, due to the fact that an electron transfers all its kinetic energy to the bremsstrahlung photon (Schönfelder, 2001).

Inverse Compton Scattering

γ-rays can also be produced when an energetic electron collides with a low energy photon. These collisions promote the photon to either become a X-ray or γ-ray photon. The typical energy of the emitted photon from such interaction is:

$$E_\gamma \simeq 1.3 \left(\frac{E_e}{(\mathrm{TeV})}\right)^2 \cdot \left(\frac{\epsilon}{2\times 10^{-4}(\mathrm{eV})}\right)(\mathrm{GeV}), \tag{2.6}$$

where ϵ is the energy of the photon before the scattering. Figure 2.8 shows a sketch of the inverse Compton scattering.

Nuclear Transitions

The atomic nuclei can be in different energy states, one can think of these states similar to the electrons quantum state in their shell. Usually the energy difference in the nuclear states flow in the MeV regime, therefore the transitions between these states requires an absorption or emission of MeV photons (γ-rays). See the schematic in figure 2.9 adapted from Schönfelder (2001).

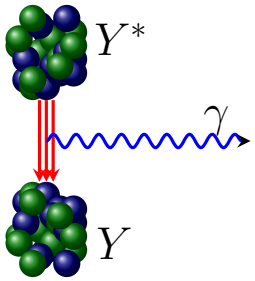

Figure 2.9: An illustration of nuclear transitions decay.

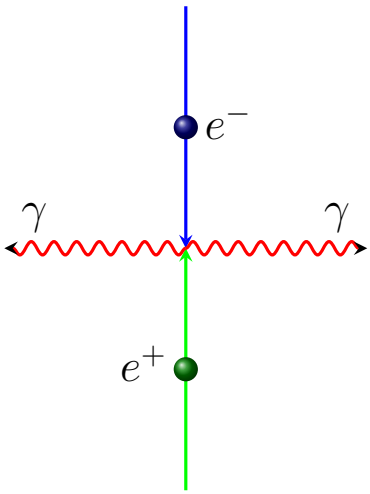

Figure 2.10: An illustration of the electric-positron annihilation.

Pion Decay

Interactions like cosmic rays (protons) colliding with the nuclei of the ambient gas can produce an extensive number of neutral and charged pions, however neutral pions (π^0) are unstable, therefore they decay into pairs of γ-ray photons (Schönfelder, 2001).

$$\pi^0 \rightarrow \gamma + \gamma \tag{2.7}$$

Annihilation

A pair of γ-ray photons can be created when a particle and antiparticle annihilate. Figure 2.10 shows a sketch of the electron-positron annihilation. Since an electron is the lightest particle with a mass of 511 KeV, the expected photons in from a electron-positron annihilation event will be in the γ-ray range.

2.2.2 Sources of GeV/TeV Gamma-ray Emission

There are two main types to the GeV/TeV γ-ray sources, galactic and extragalactic. The galactic sources can be supernova remnants, objects that remain after a supernova, i.e., black holes or neutron stars depending on the mass of the original stars. The main emission mechanism is supernova driven shock wave acceleration

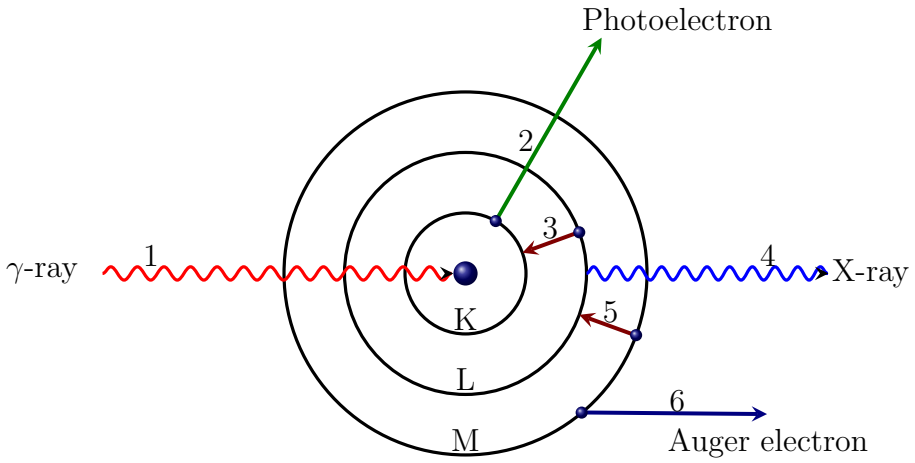

Figure 2.11: The Photoelectric Effect.

of charged particles (Malkov & O'C Drury, 2001). The other strong source of VHE γ-ray emission are pulsars which are rotating neutron stars created after a supernova explosions. VHE γ-rays are emitted from pulsars. These are produced by charged particles accelerated by the very high electric field. Inverse Compton scattering is another source of VHE. In this process, low energy photons are scattered to much higher energies by this process, which can also take place at the surface of the neutron stars (Ruderman & Sutherland, 1975; Schönfelder, 2001). Also, X-ray binary systems have been confirmed as VHE γ-ray emitters (Aharonian *et al.* , 2005b; Albert *et al.* , 2006), through synchrotron emission.

The following list summarises the known extragalactic sources for the VHE γ-ray. AGNs and starburst galaxies have been shown to emit VHE γ-rays. AGN's are powered by the gravitational energy released by the accretion onto a central supermassive black hole. Starbusrt galaxies are galaxies which show a high degree star formation activity. Observations revealed that even small starburst galaxies such as M82 are able to emit VHE γ-ray ($>$ 700GeV; VERITAS Collaboration *et al.* 2009). Another source of VHE γ-rays are Γ-ray bursts (GRBs) which are the most luminous sources in the universe with associated energies of 50keV to 1MeV (Weekes, 2003). Two different types of GRBs can be differentiated one is thought to originate from super- or hypernova explosions and the other from merging neutron stars.

2.2.3 Interaction of Gamma-rays with Matter

Photoelectric Effect

Photoelectric effect is the absorption of a photon by an electron in an atom. Different scenarios can happen depending on the energy of the absorbed photon, if the photon has sufficient energy it can release or excite the electron from its orbit. Figure 2.11 shows the different scenarios in the photoelectric interactions. This effect is the dominant interaction for low energy photons in the range between 100 eV to 100 keV.

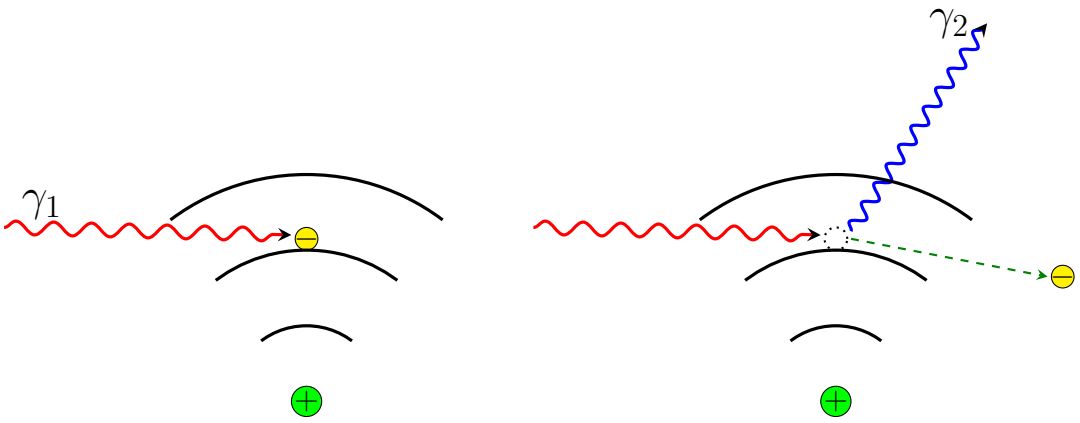

Figure 2.12: Compton Scattering.

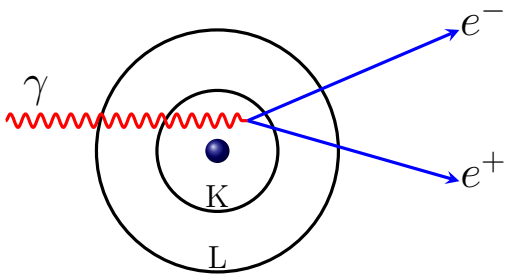

Figure 2.13: The Pair Production Effect.

Compton Effect

In this effect a photon hits a free electron and transfers some of its energy to the electron in a form of kinetic energy, and gets scattered. This interaction is dominant in the energy range of 100 eV up to MeV. Figure 2.12 provides an illustration of the scattering process.

Pair Production

When the energy of a photon is higher than the rest mass of a particle and its anti-particle the pair production interaction is allowed. The minimum energy required for the precess to occur is called a threshold energy which corresponds to two times the rest masses of the particle or, equivalently, to the sum of the rest masses of the particle and its anti-particle. This interaction happens in the presence of a strong electric fields, most likely when the high energy photon passes close to a nucleus of an atom with high atomic number. Figure 2.13 shows an illustration of this interaction.

Electromagnetic Cascades

When very high energy particles or γ-rays collide with regular matter they can generate a shower of secondary particles through pair production processes and photons with less energy through bremsstrahlung interactions. The secondary particles in the

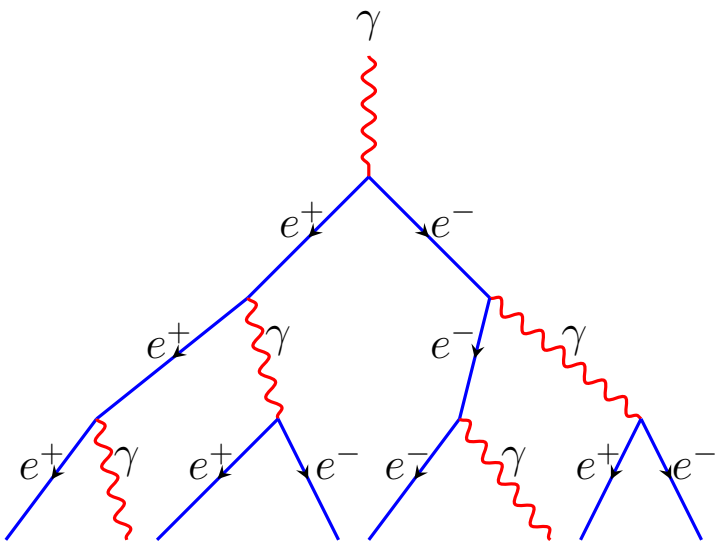

Figure 2.14: Electromagnetic Cascades.

shower emit Cherenkov radiation, which is emission due to the motion of a charged particles in non-conducting medium with speed greater than the phase speed of light in the medium. Figure 2.14 shows a schematic of electromagnetic cascading of a γ-ray.

2.2.4 Interaction of Gamma-rays with Electromagnetic Spectrum

The interaction of a high energy photon and low energy photon producing an electron-positron pair ($\gamma + \gamma' \rightarrow e^+ + e^-$) is one of the important processes that responsible of the absorption of these VHE γ-ray photons traveling from distant cosmic sources such as Quasars. This interaction can takes place only if the total energy of the two photons is higher than the rest mass of the electron-positron pair. The cross section of this interaction is the probability for the interaction to occur, and can be written as (Gould & Schréder, 1967):

$$\sigma = \frac{1}{2}\pi r_0^2(1-\beta^4)\left[(3+\beta^4)\ln\frac{1+\beta}{1-\beta} - 2\beta(2-\beta^2)\right] \tag{2.8}$$

where ($\beta = |P_e|\frac{c}{E_e} = \left(1-\frac{1}{s}\right)^{\frac{1}{2}}$) and ($E_e$) is the electron and the positron velocity and the energy at the center of mass respectively, r_0 is electron radius and $s = \frac{s_0}{2}(1-\cos\theta)$ is square energy of the center of mass and $s_0 = \left(\frac{\epsilon E}{m^2c^4}\right)$. One can see from the above equation the pair production can only occur if $s > 1$.

The optical depth (τ) is the absorption probability of energetic photons emitted at redshift z up to the observer at $z = 0$, and it can be written as (Razzaque *et al.*

, 2009):

$$\frac{d\tau_{abs}}{dx} = c\pi r_0^2 \left(\frac{m_e^2 c^4}{E}\right)^2 \int_0^z \frac{dz_1}{(1+z_1)^2} \left|\frac{dt}{dz_1}\right| \times \int_{m^2c^4/E(1+z_1)}^{\infty} d\epsilon_1 \frac{u_{\epsilon_1}}{\epsilon_1^3} \overline{\varphi}[s_0(\epsilon_1)], \tag{2.9}$$

where $\overline{\varphi}[s_0(\epsilon)] = \int_1^{s_0(\epsilon)} s\overline{\sigma}(s)ds$ and $\overline{\sigma}(s) = \frac{2\sigma(s)}{\pi r_0^2}$ with $S_0 = E(1+z)\epsilon_1/m_e^2c^4$.

The interaction of the VHE γ-ray photons and the low energy photons is the basic physical absorption that we are studying in this thesis through investigating the opacity of the VHE γ-ray photon due to the EBL photons.

2.2.5 Gamma-ray Detection

There are some challenges associated with γ-ray observations. First, the absorption probability of a 1MeV γ-ray by our atmosphere is 99.8% . This means the atmosphere is optically thick, therefore γ-rays cannot be directly observed from the surface of the Earth. Secondly, the small number of γ-ray photons compared with the number of optical photons, in other words, the cosmic γ-ray flux is very small compare with the optical flux. This is due to the fact that the amount of energy that the γ-ray photons carry can be more than million times higher than that of optical photons which obviously makes it much harder to produce the γ-rays in the first place. Therefore, there are no enough γ-rays produced in order to transfer the energy from the emitting sources. Thirdly, the background noise in γ-ray telescopes (Schönfelder, 2001).

Two different approaches can be used to detect γ-rays. The first one is using space telescopes, this is a direct approach, carried out by adopting one of the interaction processes between radiation and matter in section 2.2.3. Scintillators and pair-conversion detectors are the most commonly used detector here. The scintillator type detectors make use of a secondary electron generated by a photoelectric absorption or scattered via the Compton effect. Whereas the pair-conversion detectors measure the electron-positron pair created when high energy γ-rays (above $\sim$ 20 MeV) pass through a material with a high atomic number such as Lead or Tungsten.

The second approach is to use ground base telescopes: this approach does not directly detect γ-ray radiation, but observes the effects of the γ-ray interaction with the atmosphere. This is done by observing the Cherenkov radiation that occurs in our atmosphere due to electromagnetic cascading (see section 2.2.3).

Determination of the EBL from GeV/TeV sources

Measuring the EBL from GeV/TeV γ-ray observations works best if intrinsic spectrum of the source is known. Conversely, if the EBL is known, it can be used to determine the intrinsic spectrum of γ-ray sources and could in turn provide important constraints on the processes of VHE emission.

Different sources are used to constrain the EBL. These include blazars, a few radio galaxies, and a couple of nearby starburst galaxies detected recently. However, the majority of extragalactic γ-ray sources at VHE are blazars, therefore, the current constraints on the UV/optical to Mid-IR regions of the EBL are derived primarily from studies of blazars.

The spectra of most VHE sources follow a power-law of the form $\mathrm{dN/dE} \propto \mathrm{E}^{-\Gamma}$ over a wide energy range. The law has spectral indices Γ_{GeV} and Γ_{TeV} at GeV and TeV energies respectively. However, over sufficiently small energy ranges, there is a deviation from the power-law.

The observed spectra of blazars show a sharp cut-off between GeV and TeV energies, defined as $\Delta\Gamma_{GeV} \equiv \Gamma_{GeV} - \Gamma_{TeV}$. The location of the cut-off depends on the redshift of the source, increasing with redshift. The cause for this spectral feature is suggested to be the EBL absorption Dwek & Krennrich (2013).

A single power-law can be fitted to a VHE gamma-ray source in the region $\sim 1 - 10$ GeV which is unaffected by EBL absorption (e.g., Punch *et al.* 1992). If we assume that the intrinsic blazar spectra follow this power law to energies ~ 1 TeV, then any spectral break in the observed spectrum can be attributed to EBL absorption. In this method, spectral break analysis, the knowledge of the intrinsic blazar spectrum is not required to study the EBL.

Since different studies used different assumptions for the intrinsic spectra of the γ-ray sources, there is variation on the limits derived by this method. Nonetheless, several studies (e.g., Aharonian *et al.* 2005a; Mazin & Raue 2007; Orr *et al.* 2011) have shown that the EBL intensity at optical-IR wavelength range is close to the lower limits set by the integrated light from galaxies.

3
A New Model for EBL

In this chapter we describe the models used to generate the energy density distribution of the EBL. We used the model proposed by Razzaque *et al.* (2009) for the stellar contribution (section 3.1) while the dust contribution is modeled following the work of Finke *et al.* (2010) (section 3.2). The numerical implementations of the model developed in this thesis are discussed in section 3.3.

3.1 Razzaque Model

The Razzaque *et al.* (2009) model, hereafter referred to as (RDF09), is a forward evolution model which aims to predict the contribution of the stellar component of the EBL spectrum. It ignores the re-emission of the light in the IR of the light absorbed by dust. In this model, the starlight component ($\sim 0.1 - 10$ eV) of the EBL is inferred from the stellar thermal surface emission of main-sequence stars. This emission is modelled as blackbody radiation. The contributions from the AGNs and quasars are ignored since these objects radiate mostly in the X-ray range. Stars in the main-sequence phase are also ignored as they contribute very little in the UV-optical wavebands. Most of their emission occurs at longer wavelengths.

The RDF09 model is built as follows; if the star with M mass is born at redshift z_b and evolves away from the main-sequence at redshift $z_d(M)$, then the lifetime of this star, $t_\star$, can be written as:

$$t_\star = \int_{z_d(M)}^{z_b} dz \left| \frac{dt}{dz} \right|, \tag{3.1}$$

where,

$$\frac{dt}{dz} = \left(-H_0(1+z)\sqrt{\Omega_m(1+z)^3 + \Omega_\Lambda} \right)^{-1}, \tag{3.2}$$

H_0 is the Hubble constant, Ω_m and Ω_Λ are dimensionless matter and vacuum energy densities in the standard ΛCDM cosmology. By inverting equation 3.1 we can

determine $z_d(M)$,

$$z_d(M,z) = \\ -1+\left(-\left(\frac{\Omega_\Lambda}{\Omega_m}\right)\mathrm{sech}\left[\frac{3}{2}H_0 t_\star\sqrt{\Omega_\Lambda}+\tanh^{-1}\sqrt{1+\left(\frac{\Omega_m}{\Omega_\Lambda}\right)(1+z)^3}\right]^2\right)^{\frac{1}{3}}, \quad (3.3)$$

where,

$$t_\star = t_\odot\left(\frac{M}{M_\odot}\right)\Big/\left(\frac{L}{L_\odot}\right). \quad (3.4)$$

M and L are respectively the mass and luminosity of the main sequence star, and $M_\odot = 1.99\times10^{33}$ g, $L_\odot = 3.846\times10^{33}$ erg s^{-1} and $t_\odot \approx 11$ Gyr are the solar mass, luminosity and lifetime, respectively. Figure 3.1 shows z_d as a function of mass M, for various redshifts z, where equation (3.4) is used to approximate $t_\star$. The mass-luminosity ratio in equation (3.4) has been modeled by a single as well as a broken power law. Solid lines are based on Single Power Law (SPL; Bressan *et al.* 1993) and the dashed-lines represent the results based on a Broken Power Law (BPL; Binney & Merrifield 1998). Figure 3.1 implies that stars which are formed with masses above $10M_\odot$ leave the main sequence almost instantaneously, between $z\sim1-5$. On the contrary, stars with masses less than or equal to one solar mass stay in the main sequence for live-times close to the Hubble time.

The comoving number density of photons, dN, per comoving energy interval $d\epsilon = d\epsilon'/(1+z')$, emitted by a single star with mass M born at redshift z and integrated to the present time is given by the following expression (Razzaque *et al.* , 2009):

$$\frac{dN(\epsilon,M)}{d\epsilon} = \int_{\max\{M,z'\}}^{z} dz'\left|\frac{dt}{dz'}\right|\frac{dN(\epsilon',M)}{d\epsilon' dt}(1+z') \quad (3.5)$$

where $\frac{dN(\epsilon,M)}{d\epsilon' dt}$ is the total number of emitted photons per time par energy intervals from a star with radius R and temperature T. Assuming the radiation field of the star can be approximated as a blackbody radiator, one obtains the following expression:

$$\frac{dN(\epsilon,M)}{d\epsilon dt} = \frac{R^2}{\pi\hbar^3c^2}\frac{\epsilon^2}{\exp(\epsilon/kT)-1}, \quad (3.6)$$

where k and $\hbar$ are respectively the Boltzmanns, rationalized Planck' constants, and c is the speed of light.

The mass distribution of a given stellar population can be represented by the IMF, $\xi(M)$, given by:

$$\xi(M)\propto\begin{cases}M^{-\kappa_1} & \text{at} \quad 0.1M_\odot\le M\le M_1M_\odot,\\ M^{-\kappa_2} & \text{at} \quad M_1M_\odot\le M\le M_2M_\odot,\\ M^{-\kappa_3} & \text{at} \quad M_2M_\odot\le M\le 120M_\odot.\end{cases} \quad (3.7)$$

In the models considered here the stellar masses are constrained to a range between $M_{\min}=0.1$ and $M_{\max}=120M_\odot$ and it is assumed that the shape of the IMF does

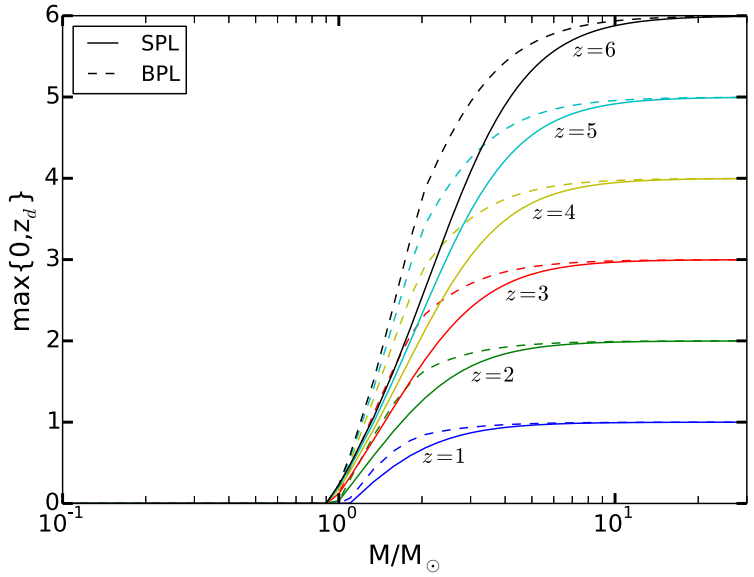

Figure 3.1: Shows $\max\{0, z_d(M, z)\}$ versus mass in solar units. This is an illustration of equation 3.3 for redshifts 1 to 6 within the standard ΛCDM cosmology. The solid lines represent the lifetime of the main sequence stars following Single Power Law (SPL) for the stellar mass-luminosity ratio (Bressan *et al.* 1993), where the dashed-lines represent results for Broken Power Law (BPL) (Binney & Merrifield 1998). (This plot is adapted from Razzaque *et al.* (2009) Fig 1).

not change with time.

Figure 3.2 shows four different IMF models deduced from observations of local galaxies which have been utilised in the models of RDF09. The heavy blue line represents the classic Salpeter IMF (Salpeter) (Salpeter, 1955). The green dashed-dotted line displays the modified Salpeter IMF (Salpeter B). The Baldry-Glazebrook IMF (Baldry & Glazebrook, 2003) is given by the red dashed line. Finally, the Scalo IMF (Scalo 1986, 1998) is shown by the cyan dashed - double dotted line. Table 3.1 lists the various parameters for these IMFs.

Table 3.1: Parameters of IMF models

IMF model	κ_1	$M_1[M_\odot]$	κ_2	$M_2[M_\odot]$	κ_3	$M_3[M_\odot]$
SalpeterA	1.5	0.5	2.35	120	-	-
SalpeterB	1.5	1.0	2.35	120	-	-
Baldry-Glazebrook	1.5	0.5	2.20	120	-	-
Scalo	1.2	1.0	2.70	10.0	2.3	120

Razzaque *et al.* (2009) considers different models for the global star formation rate (SFR), i.e. the total a amount of mass which is converted from gas into stars per unit comoveing volume and time. Those models are displayed in Figure 3.3. One

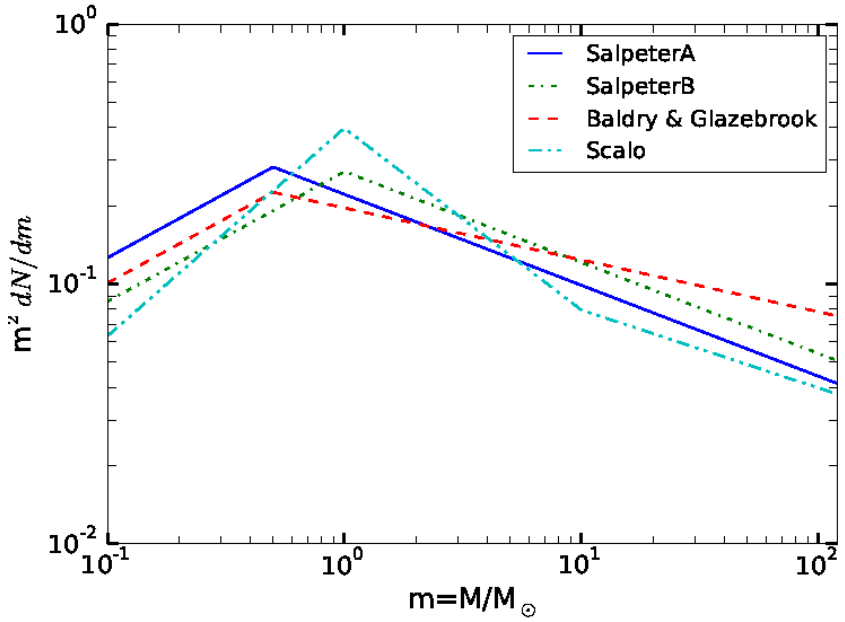

Figure 3.2: Shows four different IMFs, the blue lines shows the classic Salpeter IMF (Salpeter A; Salpeter 1955), the in green dashed - dotted is the modified Salpeter IMF (Salpeter B) , the red dashed line represents the Baldry-Glazebrook IMF (Baldry & Glazebrook, 2003) and Scalo IMF (Scalo, 1986, 1998) is displayed as cyan dashed - double dotted line. (This plot is adapted from Razzaque *et al.* (2009) Fig 2).

such model follows Cole *et al.* (2001) by assuming that the SFR has a functional form given by:

$$\psi(z) = \frac{h(a+bz)}{[1+(z/c)^d]}, \tag{3.8}$$

where the values for a, b, c and d are given in table 3.2. The table also introduces the denotation of the different models from A through E as used by Razzaque *et al.* (2009). Another model adapted from Hopkins & Beacom (2006) assumes that the SFR has the following functional form:

$$\psi(z) = \begin{cases} 10^a(1+z)^b & \text{at} \quad 0 \le z \le z_1 \\ 10^c(1+z)^d & \text{at} \quad z_1 \le z \le z_2 \\ 10^e(1+z)^f & \text{at} \quad z_2 \le z \le 6. \end{cases} \tag{3.9}$$

The values for a, b, c, d, e and f are given in table 3.2 (for the models D and F). Figure 3.3 displays the different SFRs as a functions of redshift. The SFRs for the models A through E are given by the blue (dashed), the green, the red (dashed-double dotted), the cyan (dashed) and the purple (dashed-dotted) lines, respectively.

It is evident that the shape and the amplitude of the global SFR and the IMF (discussed above) have a strong impact on the shape and amplitude of the EBL.

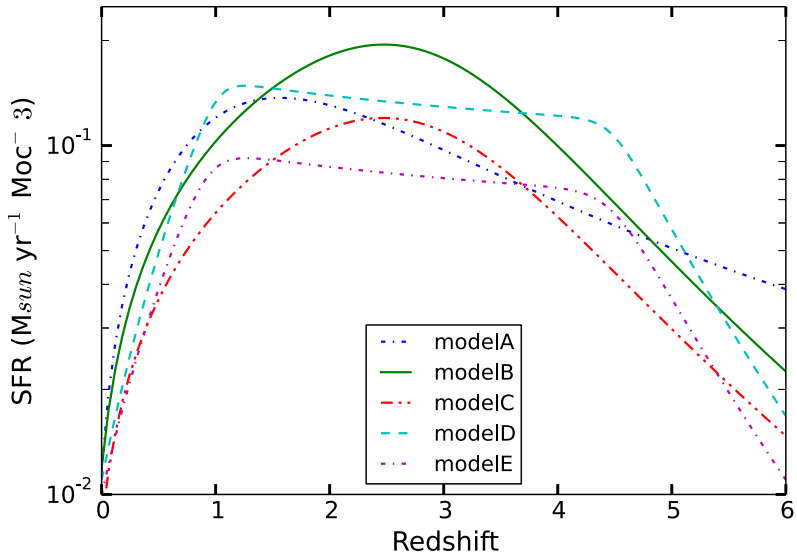

Figure 3.3: Shows five different SFR models. Where the blue dashed-line is model A, the green line is the model B, the red dashed double dots is model C, the cyan dashed line is model D and the model E in purple dashed-dot line. (This plot is adapted from Razzaque *et al.* (2009) Fig 3).

Table 3.2: Parameters of SFR models

model	IMF model	a	b	c	d	e	f	z_1	z_2
A	Salpeter A	0.0166	0.18	1.9	2.6	-	-	-	-
B	Salpeter B	0.0170	0.13	3.3	5.3	-	-	-	-
C	BaldryGlazebrook	0.0118	0.08	3.3	5.2	-	-	-	-
D	Salpeter B	-1.82	3.28	-0.724	-0.26	4.99	-8.0	1.04	4.48
E	BaldryGlazebrook	-2.02	3.44	-0.930	-0.26	4.67	-7.8	0.97	4.48

A, B and C are used for equation 3.8, D and E are used for equation 3.9.

Razzaque *et al.* (2009) computed the spectral energy density of the EBL using:

$$\frac{dN(\epsilon, z=0)}{d\epsilon dV} = \mathcal{N} \int_{z=0}^{\infty} dz'' \left|\frac{dt}{dz''}\right| \psi(z'') \int_{M_{\min}}^{M_{\max}} dM \xi(M) \times \int_{\max\{0, z_d(M,z')\}}^{z"} dz' \left|\frac{dt}{dz'}\right| f_{esc}(\epsilon') \frac{dN(\epsilon', M)}{d\epsilon' dt}(1+z'), \quad (3.10)$$

where $\mathcal{N}^{-1} = \int_{M_{\min}}^{M_{\max}} dM \xi(M)$ is the IMF normalization factor, and $f_{esc}(\epsilon')$ is an empirical fitting function for the averaged photon escape fraction from the galaxy (adapted from Driver *et al.* (2008)). As mentioned above, the optical and UV photons which are absorbed by dust are re-emitted in the IR. This process will be treated in more detail when the work by Finke *et al.* (2010) is discussed. By multiplying equation 3.10 by ϵ^2 the energy density, ϵu_ϵ, can be obtained. Consequently,

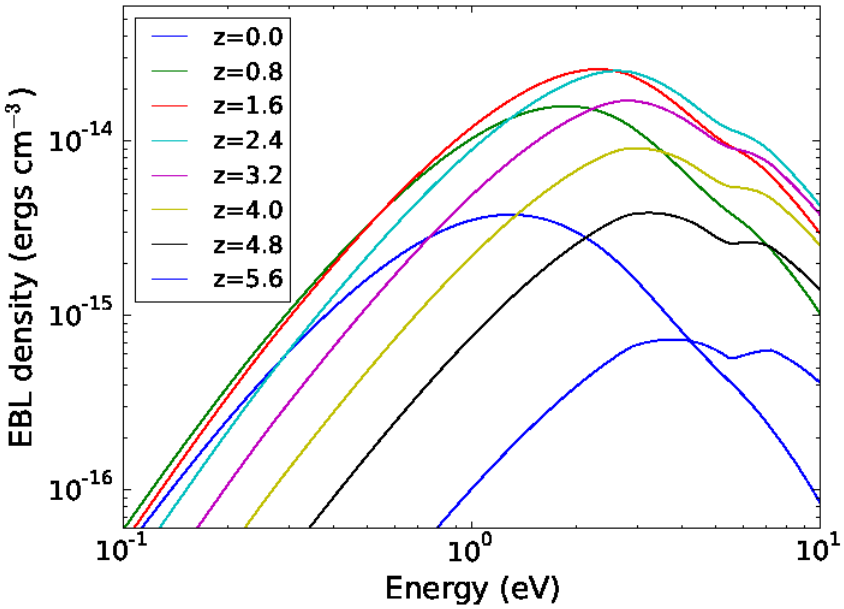

Figure 3.4: The EBL energy density obtained by Razzaque *et al.* (2009) modelling at different redshifts, using Model-B as described in table 3.2 with SPL approximation.

the comoving EBL density is given by equation:

$$\epsilon u_\epsilon = (1+z)^4 \epsilon^2 \frac{dN(\epsilon, z)}{d\epsilon dV} \tag{3.11}$$

Figure 3.4 shows the EBL energy density for various redshifts based on RDF09 model B.

3.2 Finke Model

The model of Finke *et al.* (2010), hereafter referred to as (FRD10), is an extension of the RDF09 model with the aim to predicting the EBL for wavelengths up to 1000 μm. As mentioned in chapter 2, dust absorbs radiation from stars and remits it at longer wavelengths. In the FRD10 model the full EBL spectrum is constructed by adding a model for the dust re-emission process.

The FRD10 dust re-emission model is based on the empirical dust model by Desert *et al.* (1990). FRD10 used three components for the dust in the ISM, big and very small grains and polycyclic aromatic hydrocarbons (PAHs; Desert *et al.* 1990). The big grains are the coolest with a temperature around 40 K. Therefor this component re-emits in the far-IR. The small grains with a temperature around 70 K are expected to emit at near-IR wavelength. Finally, the PAHs have temperatures of some 450 K and could emit broad emission lines, and generally PAHs are not in thermodynamic equilibrium with their environment (Dwek *et al.* , 1997). The temperatures of the different dust species and the fractional contribution to the re-emission spectrum are presented in table 3.3.

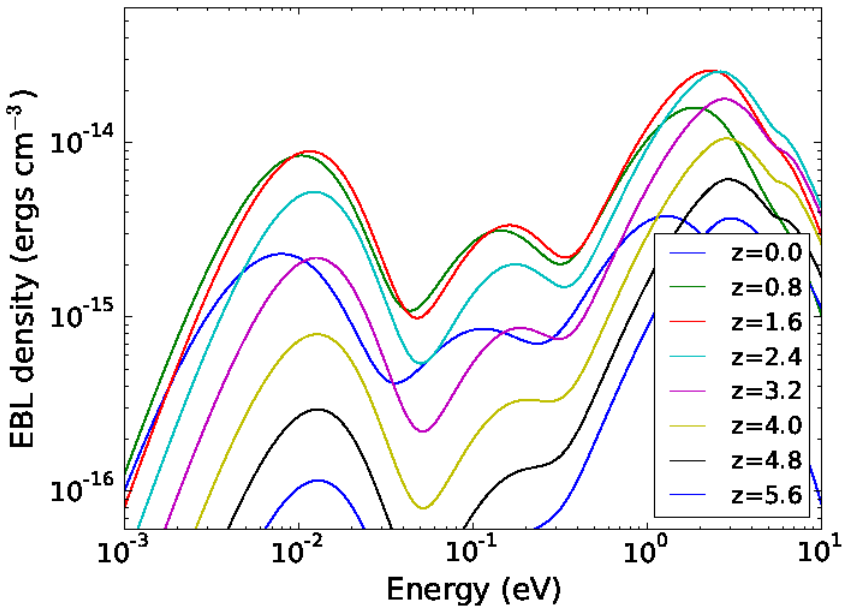

Figure 3.5: The EBL energy density based on the Finke *et al.* (2010) model at different redshifts, using model-B as described in table 3.2 with SPL approximation for the stellar mass - luminosity relation.

The FRD10 model assumes that the dust contributions can be represented by a combination of three blackbody spectra (BB), each one represents a different type of dust. To determine the fractional contribution of each dust component, Finke *et al.* (2010) fitted the observed IR luminosity data at $z = 0.0$ and $z = 0.1$. The proper luminosity density ϵL_ϵ was calculated using the following equation:

$$\epsilon L^{dust}(\epsilon_1, z) = \frac{15}{\pi^4} \int d\epsilon \left[\frac{1}{f_{esc}(\epsilon)} - 1\right] L^{stars}(\epsilon_1, z) \times \sum_{n=1}^{3} \frac{f_n}{(kT_n/m_e c^2)^4} \frac{\epsilon^4}{\exp[m_e c^2 \epsilon / kT_n] - 1}. \quad (3.12)$$

where $\left[\frac{1}{f_{esc}(\epsilon)} - 1\right] L^{stars}$ is the fraction of energy absorbed by the dust. f_n and T_n are respectively the fraction and the temperature of each dust component in the ISM and $n = 1, 2, 3$. The values for these parameters are presented in table 3.3. L^{stars} is the luminosity density escaped from the stars derived in RDF09 (Finke *et al.* , 2010).

Figure 3.5 shows the EBL densities at different redshifts obtained using a combination of the RDF09 and the FRD10 approaches. The RDF09 approach is used to compute the comoving EBL density and from the FRD10 approach the dust re-emission description is adapted.

3.3 Numerical Implementation

The ultimate goal of this work is to investigate the impact of the EBL fluctuations on the VHE γ-ray spectra from distant blazars. To do this, we started by calculating

Table 3.3: Dust parameters from FRD10. n, f_n and T_n° are the dust label, fractions and temperatures respectively.

Dust Component	n	f_n	T_n° [K]
Warm large grains	1	0.60	40
Hot small grains	2	0.05	70
PAHs	3	0.35	450

the EBL spectrum energy distribution based on models proposed by Razzaque *et al.* (2009) and Finke *et al.* (2010). However, unlike their models, the spectrum generated here covers the energy range from 0.001 to 100 eV using 400 logarithmically scaled sampling points. In order to compute the optical depth for VHE γ-rays from distant sources which requires an integration along the path of the γ-rays, the EBL spectrum has to be known as a function of redshift. We therefore computed the EBL spectrum for the redshifts from 0 to 10 using 1000 steps.

Due to the nested integrals in equation 3.10 the computational effort to determine a single EBL spectrum at a given redshift is substantial. It takes about 20 minutes to compute one spectrum. Consequently, the computation of 1000 spectra would take two weeks. We therefore used a parallel computing strategy, based on the use of shell scripts, this reduced the run time to 2 days.

In our new model, fluctuations in the EBL are implemented by means of fluctuations in the SFR density. The rationale behind this approach is that, if a region shows a low SFR for some time, the galaxy population density is lower compared to the cosmic mean. It is self-evident that such regions may show lower EBL intensities simply because there is a smaller number of galaxies in this region.

It is very difficult to extract spatial fluctuations of the SFR from observations, i.e. from large galaxy catalogues such as Sloan Digital Sky Survey (SDSS; Spergel *et al.* 2007) or the 6-degree Field survey (6DF) (Jones *et al.* , 2004) or Two Micron All-Sky Survey (2MASS) (Skrutskie *et al.* , 2006). Therefore, in this work we estimate the fluctuations of the SFR from the publicly available, semi-analytical galaxy catalogue by Guo *et al.* (2013) based on the Millennium Run 7 ($MR7$) (Lemson & Virgo Consortium, 2006). MR7 is a large cosmological N-body simulation which was set up to study the structure evolution of dark matter (Guo *et al.* , 2013). The simulation uses a specially customized version of the GAlaxies with Dark matter and Gas intEracT 2 (GADGET2) which is based on a "TreePM" solver (Lemson & Virgo Consortium, 2006). This method – used for evaluating gravitational forces – is a combination of a classical Fourier transform particle-mesh method and the Tree algorithm.

The MR7 run computes the evolution of 2160^3 dark matter particles, i.e. dark matter phase space elements, with masses of $m_p = 8.61 \times 10^8 M_\odot$ in a box of 500 Mpc/h on a side from redshift $z = 50$ to $z = 0.0$. Based on 62 snapshots from MR7 run the merger trees were extracted and used to generate semi-analytic galaxy catalogues (Guo *et al.* , 2013) which have been proven to result in observed properties that are derived from large galaxy catalogues such as mass function and color dis-

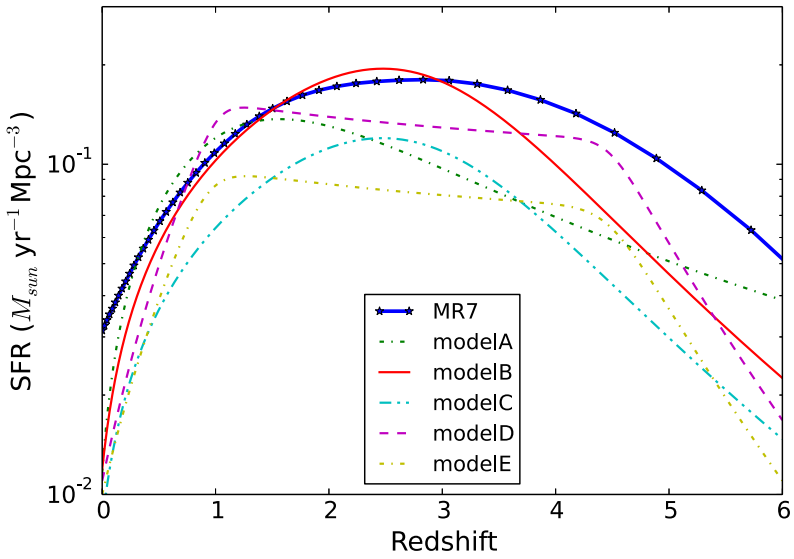

Figure 3.6: Mean SFR derived from the Guo et al. (2013) galaxy catalogue based on the MR7 (solid blue line). The redshifts of the available snapshots are indicated by the black stars. The other lines show the models presented in Figure 3.3.

tribution. The good statistical agreement between modeled galaxies and observed ones allows us to derive the fluctuations in the SFR from the semi-analytical catalogues rather than from the observed ones. Figure 3.6 shows the mean SFR derived from the Guo *et al.* (2013) galaxy catalogue as solid blue line where the black stars represent the redshifts of the available snapshots.

As mentioned above, the Millennium data base is a public data base which can be queried via a web portal based on the Structured Query Language (SQL). Figure 3.7 shows an example query to retrieve the stellar mass, SFR, positions and masses of the Guo *et al.* (2013) galaxy catalogue. At $z = 0$ the catalogue comprises about 30 Million galaxies. Such large amounts of data can not be downloaded via a graphical user interface (GUI). Therefore, the query has been incorporated in a shell script allowing one to circumvent the GUI and to download directly the data from the data base. Even with this approach, the data for a single snapshot can not be retrieved as a single big file. The data have to be separated into smaller chunks in order to make the transfer via the Internet feasible. This is why the Peano-Hilbert key (PHkey) is used in the query. The Peano - Hilbert curve is a space filling curve which is used as parameter (or key) to select swiftly only those galaxies which are located in close proximity. Therefore, working successively through the entire range of the PHkey $(1 - 16777214)$ allows one to gradually retrieve all galaxies in the simulation box.

Scatter of the SFR

To compute the mean as well as upper and lower limits of the scatter for the SFR we employed the following steps:

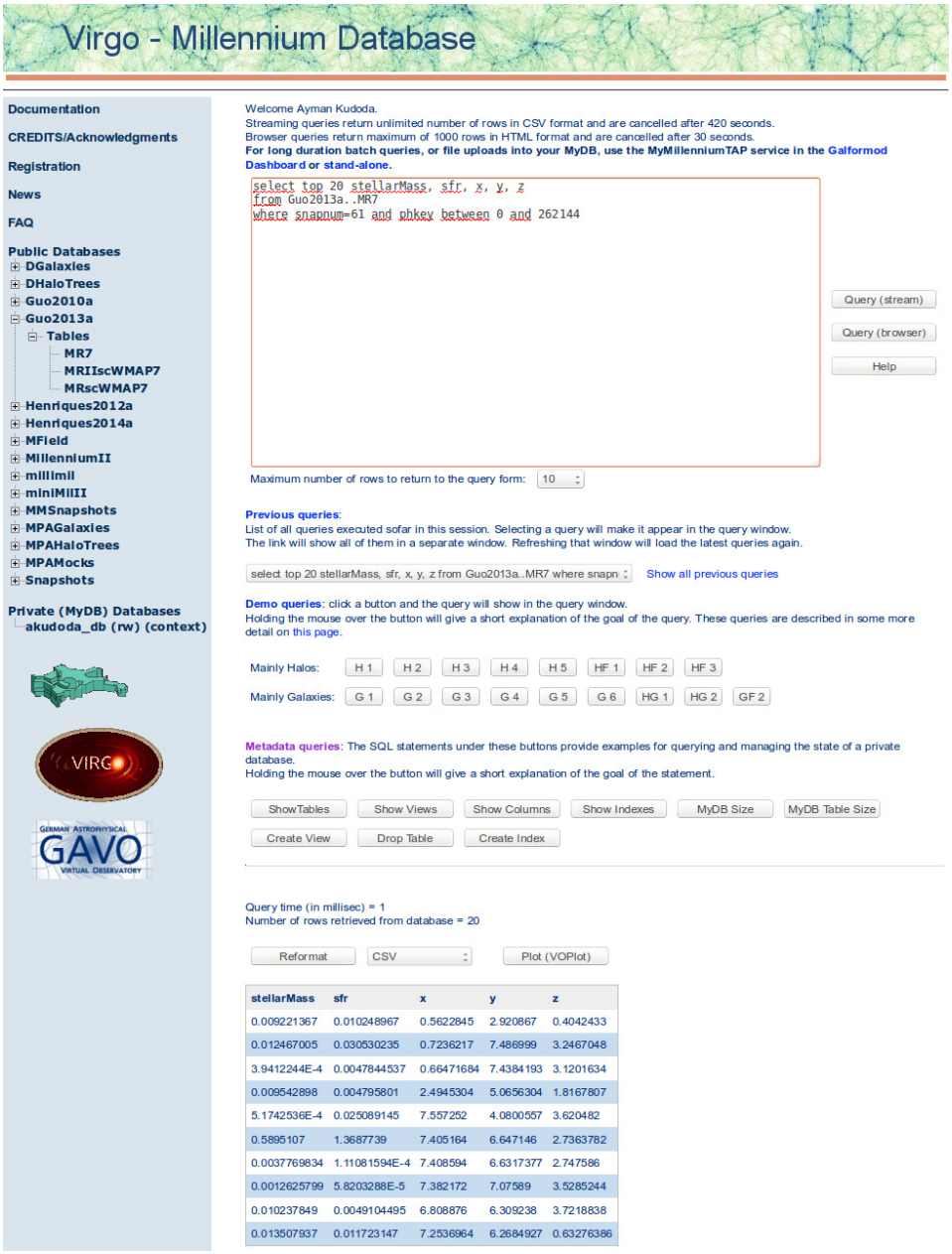

Figure 3.7: SQL query to retrieve stellar mass, SFR and position of Guo et al. (2013) galaxies. Screen shot taken for the Millennium web-page showing an SQL sequence similar to that used in the script for obtaining the star formation rates.

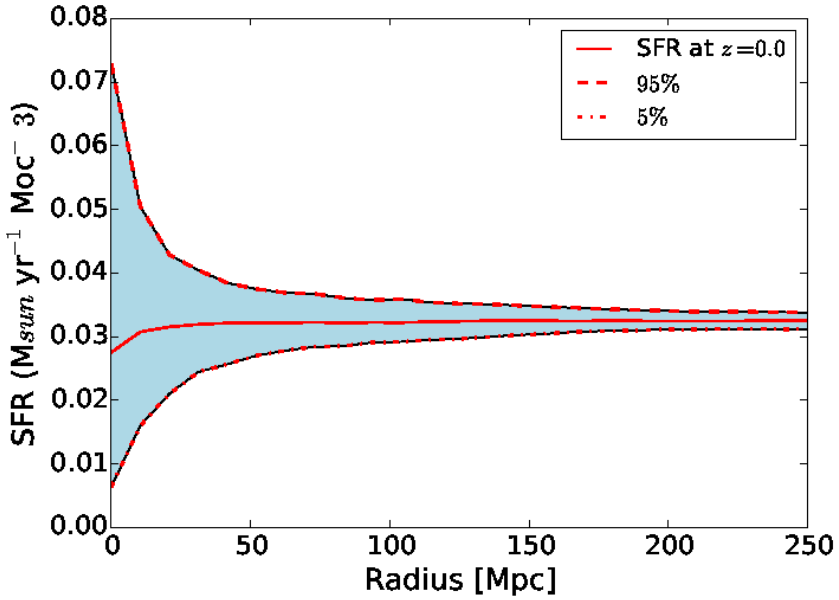

Figure 3.8: The SFR radial profile at redshift 0.0 where the solid red line is the mean SFR density, the dashed and dashed doted red lines are the upper and lower limits respectively.

- We choose 1000 points of a 3D ($10 \times 10 \times 10$) grid in an MR7 simulation box with separation of 50 Mpc between points.
- For a chosen point on the grid, we applied periodic boundary conditions to centralize the point and created 25 shells around it, resulting in a shell thickness of 10 Mpc.
- For each shell we computed the average SFR density thus creating a radial profile.
- We repeated the second and third steps for the 1000 grid points.
- Then we computed the upper limit of the scatter as 95 %, mean and the lower limit of the scatter as 5 % of the 1000 radial SFR density profiles. Figure 3.8 shows an example of the mean SFR for each shell, where the shaded "trumpet" shaped area represents the upper and lower limits of the SFR at $z = 0.0$.
- We repeated the above steps for the 62 available snapshots (the first galaxies appear in snapshot ~ 7).
- We then converted the shell radii, $R_{\rm i}$, to a redshift, $z_{\rm i}$, by using the distance-redshift relation, $z_{\rm i} = H(z) \times R_{\rm i} * a(z)$, where $H(z)$ and $a(z)$ are the Hubble parameter and the scale factor at redshift of the snapshot.

Once the mean, and lower and upper limits for the scatter of the SFR were determined, we implemented these limits in equations 3.10 and 3.12 to find the mean, lower and upper limits of the EBL spectrum.

Gamma-ray Opacity Calculation

The interaction of the EBL with γ-rays can create opacity for the propagating GeV/TeV photons due to an electron-positron pair formation. Determining the opacity of the Universe to the γ-rays is important for several VHE γ-ray observations such as the Fermi γ-ray Space telescope and High Energy Stereoscopic System (H.E.S.S).

Therefore, we derived the γ-ray opacity with upper and lower limits by inserting the mean, the upper and lower EBL energy densities obtained above, into equation 2.9 accordingly, in the energy range of 0.1 to 1 Tev.

The above calculations require substantial computations. We were able to speed up the process by using logarithmic sampling points in the integrations, which allowed us to reduce the number of sampling points without reducing accuracy, and parallel processing where it was applicable. For instance, to compute the EBL spectrum, the job was distributed among 12 cpus which allowed us obtain the results after several days of computation.

4 Results

4.1 Fluctuations in the Star Formation History

As discussed in section 3.3 we derived the fluctuations in the SFR for the 62 MR7 snapshots. Figure 4.1 shows the global SFR history with the upper and lower limits for each snapshots up to redshift 6. From this figure we can clearly see that the SFR profiles share the same "trumpet" like shape. A comparison of the shape of functional form revealed that they are almost identical. Figure 4.2 shows an example of the normalized SFR radial profile for 6 different snapshots obtained using the mean SFR density profile at each snapshot as a normalization factor. Furthermore, we can also deduce from this figure that the value of the SFR density fluctuates strongly ($\pm 50\%$ off the mean density) when the volume is smaller, for example strong differences in the mean SFR are observed in spheres with radius less than 25 Mpc, for larger volumes, i.e. for shells with larger radii, the differences are small. This is expected since the SFR averaged over large volumes should approach the cosmic mean.

This findings imply that the EBL at a given redshift may deviate from the cosmic average at that time due to the local variation of the SFR, i.e. in extreme cases the integration backwards in time to obtain the EBL spectrum (Equation 3.10) starts at the upper edge of the trumpet or the lower one. But these differences quickly reduce as the integration progresses to larger redshifts and therefore spheres with larger radii. To calculate the intensity of the γ-rays (radiation) after they have propagated through the EBL, we need to integrate the interaction probability of the γ-rays with the EBL over the redshift range corresponding to the distance of the γ-ray source. In order to determine a lower or upper limit for the optical depth of the γ-rays we will use respectively the lower or upper edges of the trumpets for entire redshift range of the integration.

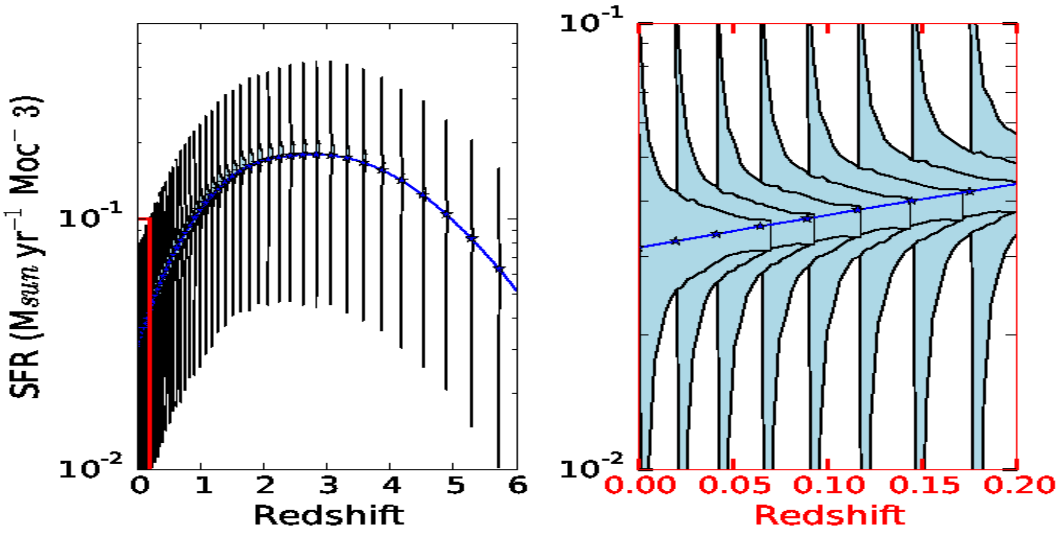

Figure 4.1: Left panel: the SFR history derived from MR7 with the fluctuations from each snapshots as vertical "bulgy-strips". Right panel: enlargement of region shown in red in the left panel. Because of their shape, we shall call them "trumpets".

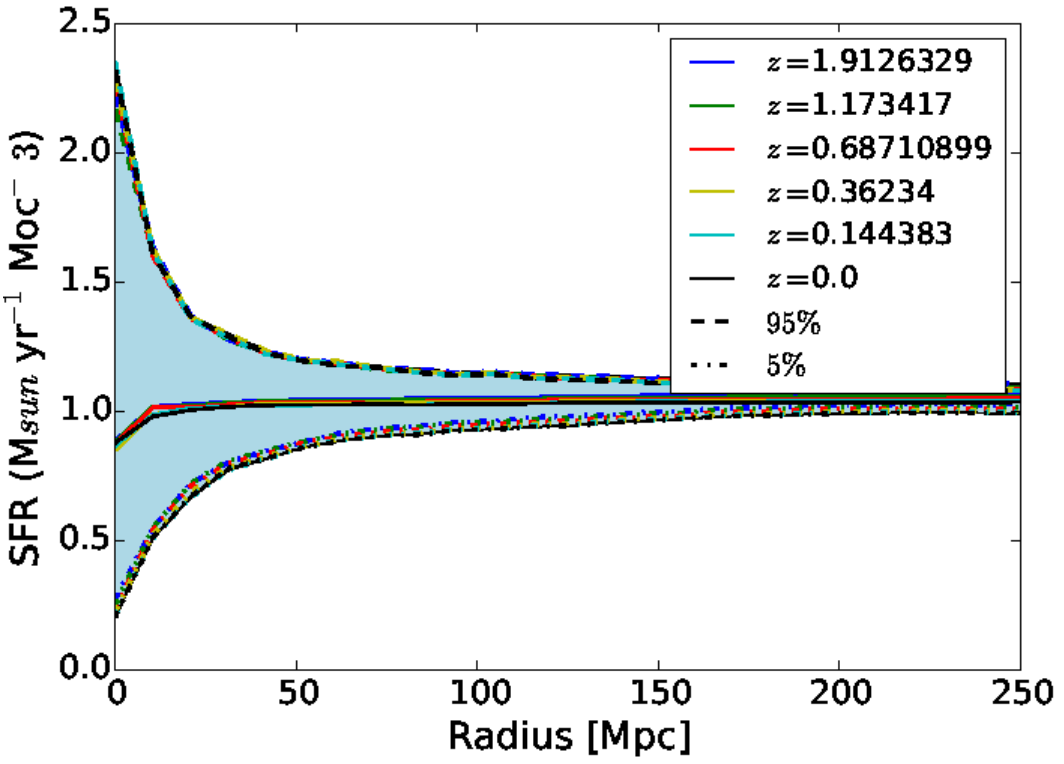

Figure 4.2: Six overlapping trumpets at different redshifts. This figure shows clearly that the shape of the SFR fluctuations as a function of redshift is nearly independent of redshift.

4.2 Upper and Lower Limits of the EBL Density

Reproducing the EBL model proposed in Razzaque *et al.* (2009) for the stellar EBL component, and following Finke *et al.* (2010) approach for the dust emission, we extended the spectrum to 100 eV. The trumpets discussed in Section 4.1 are all nearly identical in shape. We used this fact to fit the upper and lower EBL limits for the snapshots up to redshift 6 using two suitable functional forms. Inserting these fitting functions in to our EBL model, we obtained the mean, upper and lower EBL densities. Figure 4.3 shows the EBL spectrum for different redshifts ($z = 0$, 2, 4 and 6).

4.3 Upper and lower Limits of Gamma-ray Opacity

Figure 4.4 shows the γ-ray optical depth based on Equation 2.9 (In the following, optical depth and opacity are used interchangeably) for observed energies, E_γ, and different redshifts in the energy range of 0.1 to 1 eV. We can see that at higher redshifts (above $z \sim 5$) the higher γ-ray energies (above $E_\gamma \sim 50$ GeV) opacities are almost identical. The inclusion of the dust re-emission spectrum allows us to investigate the total EBL spectrum from 0.01 up to 100 eV. Therefore we were able to include a wider γ-ray energy range, from 1 up to 1000 GeV (compared to Razzaque *et al.* 2009). Nonetheless, it is assuring that our γ-ray opacity calculations matched those presented in Razzaque *et al.* (2009) for the corresponding energy range.

In this work, we investigated two extreme scenarios to determine the upper and the lower γ-ray opacity limits. One extreme is the scenario where we assumed that the γ-ray is traveling through over dense regions all the way form the source at a given redshift z up to redshift $z_o = 0.0$. The other scenario is where the γ-ray traveling through under dense regions from the source at the redshift z up to the redshift $z_o = 0.0$.

The final result of this approach is presented in Figure 4.5, where the impact of the fluctuations in the EBL on the γ-ray opacity or optical depth is shown. The figure displays the upper and lower percentage limits of the opacity at different redshifts. From this Figure, we see clearly that the opacity can vary significantly at lower redshifts (e.g., $z \sim 0.5$ the variation is about 35% from the mean), but as we go to larger redshifts the impact of the fluctuation decreases. However, the impact of the fluctuation on the VHE γ-rays is relatively small, $\pm 2\%$ at the energies above 100 GeV. These results are in good agreement with the results derived by Furniss *et al.* (2015).

For low energy γ-rays, the EBL is transparent, i.e. the optical depth approaches zero. Accordingly, we see the extreme increase for γ-rays approaching low energies (the lower part of Figure 4.5), and decreases for γ-rays approaching low energies(the top part of Figure 4.5). The fact that the extremes are located at lower energies for higher redshifts is a result of the redshifting of the *gamma*-ray energy. Focussing on the horizontal parts of the graphs in Figure 4.5, we find that the difference between γ-rays traveling though under-luminous regions as compared to those traveling though over-luminous regions amounts to approximately $\leq 15\%$ which may have a measurable impact on the shape of the high energy part of γ-ray spectra.

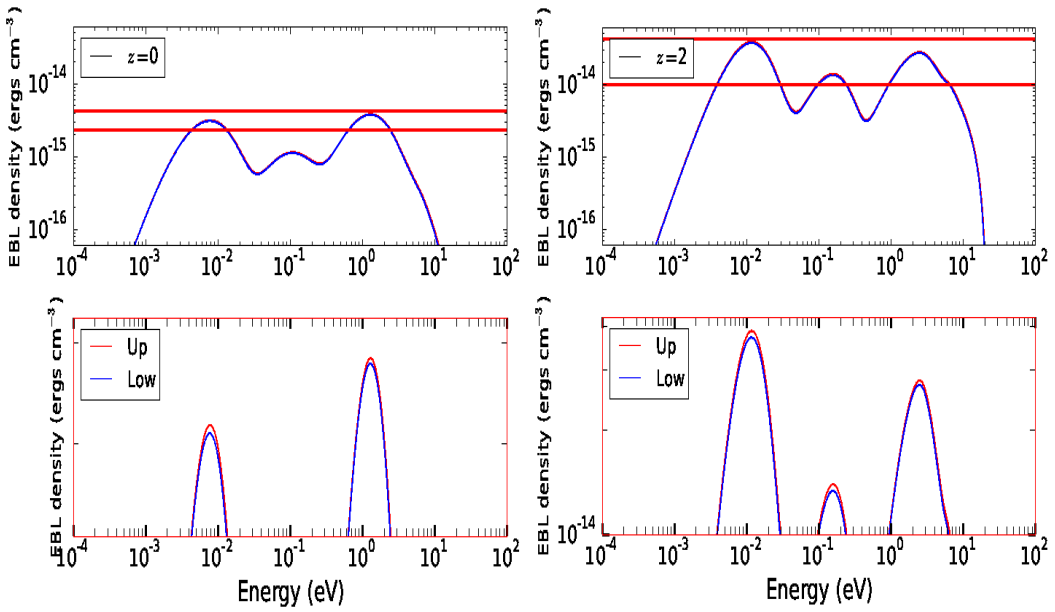

(a) $z = 0$

(b) $z = 2$

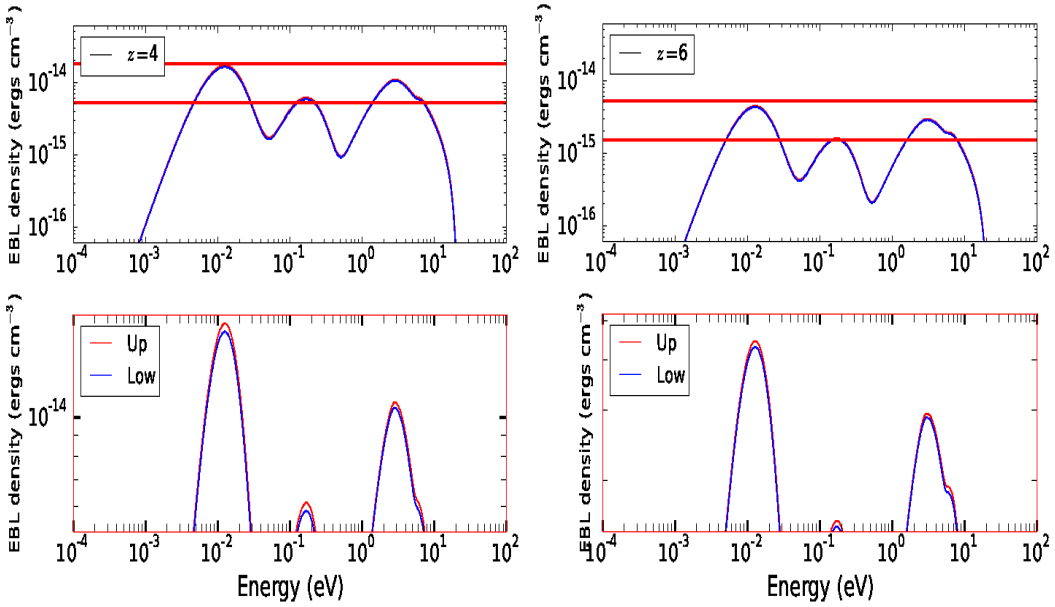

(c) $z = 4$

(d) $z = 6$

Figure 4.3: The EBL energy density for Model B described in section 3.1 for different redshifts from 0.001 to 100 eV. In order to show the difference between the upper and lower limits of the EBL density, the lower panels present enlarged views of the regions between the red lines on the corresponding upper panels.

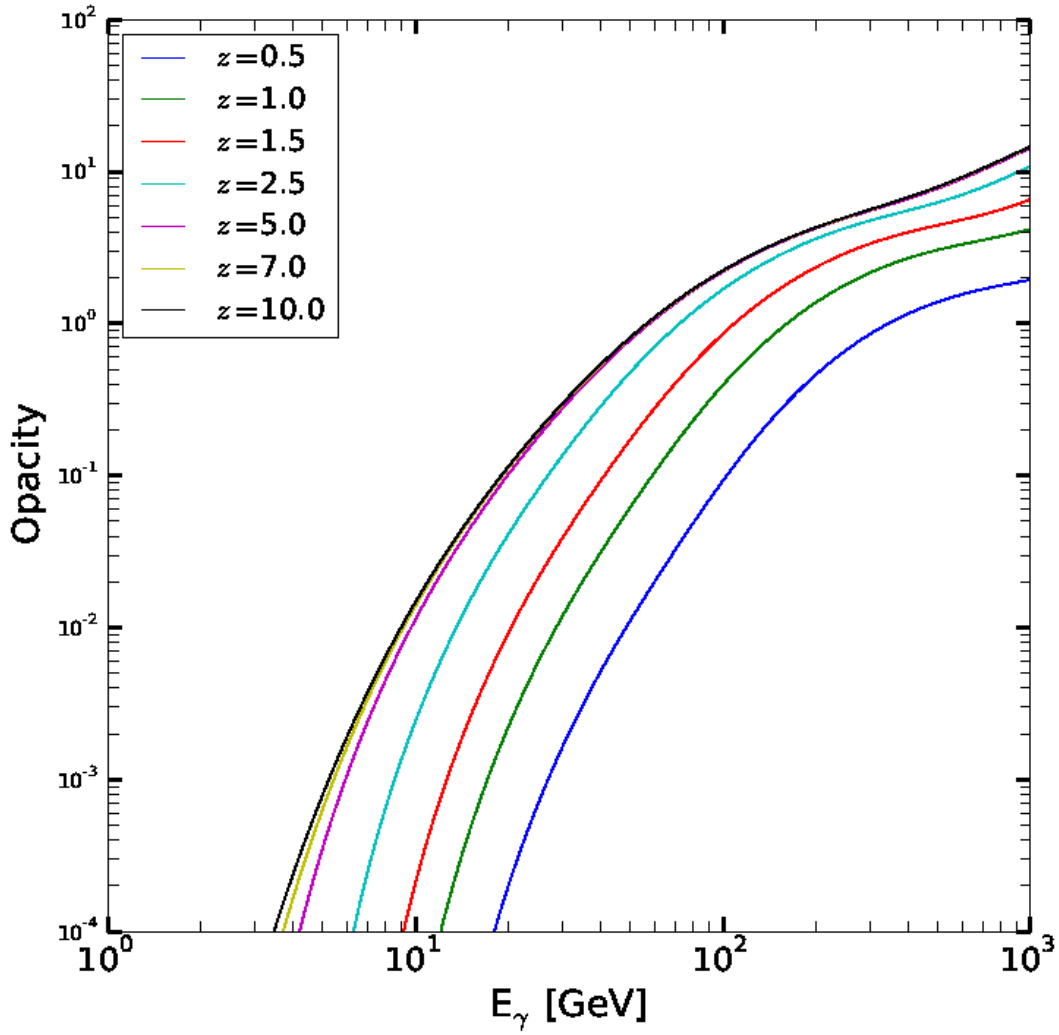

Figure 4.4: Gamma-ray opacity of the Universe at different redshifts, with energy range of 0.1 to 1 TeV. With observed energy, E_γ, and for increasing redshifts, 0.5 to 10, from inner to outer lines.

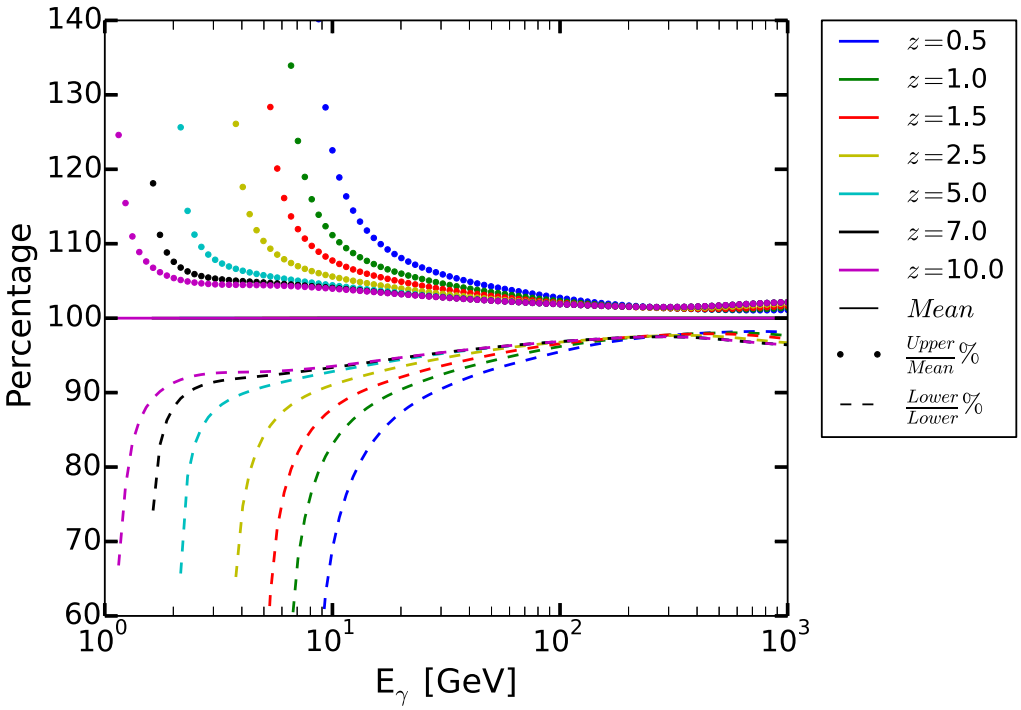

Figure 4.5: The difference between the γ-ray opacity and its upper and lower limits in percentage as a function of observed γ-ray energy, E_γ. The doted and the dashed lines are the upper and lower limits. The graphs for all redshifts show a strong increase of the deviation from the mean when the observed energies, E_γ, approach a lower energy limit (from the top). This is a consequence of the (mean) optical depth approaching zero for low γ-ray energies. However, the horizontal part of the graphs indicate a relative difference of $\leq$15%, which should be sufficient to have an impact on the shapes of the high energy parts of γ ray depending of whether the rays predominantly encountered over or under-luminous regions.

5 Conclusions

Understanding the evolution of the EBL is crucial for understanding γ-ray astronomy, and for galaxy evolution in general. We reproduced the Razzaque *et al.* (2009) model which determined the stellar component of the EBL spectrum, and extended their work following the work by Finke *et al.* (2010) to include the dust component of the spectrum. For that purpose, we have developed and optimised our code in order to predict realistic EBL spectra at minimum of computational cost.

As a new feature, we introduced fluctuations in our EBL model. The fitting function for the scatter of the EBL was based on the fluctuations in the SFR density observed in the Guo *et al.* (2013) galaxy catalogue. Our results show that the fluctuations of the SFR density in the smaller volumes (less than 25 Mpc sphere radius) can reach up to $\pm 50\%$ off the mean density.

The upper and lower limits of the EBL density fluctuations determined at different redshifts were used to compute the impact of the fluctuation on the γ-ray optical depth. To the best of our knowledge, this is the first detailed analytical model aiming to account for the impact of EBL fluctuations on the γ-ray opacity. Our model predicts relatively high variations ($\leq 15\%$) on the opacity in the energy range less than 100 GeV for nearby sources, whereas the impact is found to be smaller, $\sim 5\%$, for VHE γ-rays from distant sources.

Future Perspectives

In the future we plan to carry out further investigations on the subject and run full 3D simulations to obtain a better under- standing of the EBL fluctuations and their relation to observed γ-ray spectra. With an eye to the Cherenkov Telescope Array (CTA) and other future γ-ray observations and galaxy surveys, the measurement of the EBL fluctuation may prove to be a powerful tool in cosmology for obtaining insight into the workings of our Universe.

Bibliography

Ackermann, M., Ajello, M., Allafort, A., Schady, P., Baldini, L., Ballet, J., Barbiellini, G., Bastieri, D., Bellazzini, R., Blandford, R. D., Bloom, E. D., Borgland, A. W., Bottacini, E., Bouvier, A., Bregeon, J., Brigida, M., Bruel, P., Buehler, R., Buson, S., Caliandro, G. A., Cameron, R. A., Caraveo, P. A., Cavazzuti, E., Cecchi, C., Charles, E., Chaves, R. C. G., Chekhtman, A., Cheung, C. C., Chiang, J., Chiaro, G., Ciprini, S., Claus, R., Cohen-Tanugi, J., Conrad, J., Cutini, S., D'Ammando, F., de Palma, F., Dermer, C. D., Digel, S. W., do Couto e Silva, E., Domínguez, A., Drell, P. S., Drlica-Wagner, A., Favuzzi, C., Fegan, S. J., Focke, W. B., Franckowiak, A., Fukazawa, Y., Funk, S., Fusco, P., Gargano, F., Gasparrini, D., Gehrels, N., Germani, S., Giglietto, N., Giordano, F., Giroletti, M., Glanzman, T., Godfrey, G., Grenier, I. A., Grove, J. E., Guiriec, S., Gustafsson, M., Hadasch, D., Hayashida, M., Hays, E., Jackson, M. S., Jogler, T., Kataoka, J., Knödlseder, J., Kuss, M., Lande, J., Larsson, S., Latronico, L., Longo, F., Loparco, F., Lovellette, M. N., Lubrano, P., Mazziotta, M. N., McEnery, J. E., Mehault, J., Michelson, P. F., Mizuno, T., Monte, C., Monzani, M. E., Morselli, A., Moskalenko, I. V., Murgia, S., Tramacere, A., Nuss, E., Greiner, J., Ohno, M., Ohsugi, T., Omodei, N., Orienti, M., Orlando, E., Ormes, J. F., Paneque, D., Perkins, J. S., Pesce-Rollins, M., Piron, F., Pivato, G., Porter, T. A., Rainò, S., Rando, R., Razzano, M., Razzaque, S., Reimer, A., Reimer, O., Reyes, L. C., Ritz, S., Rau, A., Romoli, C., Roth, M., Sánchez-Conde, M., Sanchez, D. A., Scargle, J. D., Sgrò, C., Siskind, E. J., Spandre, G., Spinelli, P., Stawarz, Ł., Suson, D. J., Takahashi, H., Tanaka, T., Thayer, J. G., Thompson, D. J., Tibaldo, L., Tinivella, M., Torres, D. F., Tosti, G., Troja, E., Usher, T. L., Vandenbroucke, J., Vasileiou, V., Vianello, G., Vitale, V., Waite, A. P., Winer, B. L., Wood, K. S., & Wood, M. 2012. The Imprint of the Extragalactic Background Light in the Gamma-Ray Spectra of Blazars. *Science*, **338**(Nov.), 1190–.

Aharonian, F., Akhperjanian, A. G., Aye, K.-M., Bazer-Bachi, A. R., Beilicke, M., Benbow, W., Berge, D., Berghaus, P., Bernlöhr, K., Boisson, C., Bolz, O., Borrel, V., Braun, I., Breitling, F., Brown, A. M., Gordo, J. B., Chadwick, P. M., Chounet, L.-M., Cornils, R., Costamante, L., Degrange, B., Dickinson, H. J., Djannati-Ataï, A., Drury, L. O., Dubus, G., Emmanoulopoulos, D., Espigat, P., Feinstein, F., Fleury, P., Fontaine, G., Fuchs, Y., Funk, S., Gallant, Y. A., Giebels, B., Gillessen, S., Glicenstein, J. F., Goret, P., Hadjichristidis, C., Hauser, M., Heinzelmann, G., Henri, G., Hermann, G., Hinton, J. A., Hofmann, W., Holleran, M., Horns, D., Jacholkowska, A., de Jager, O. C., Khélifi, B., Komin, N., Konopelko, A., Latham, I. J., Le Gallou, R., Lemière, A., Lemoine-Goumard, M., Leroy, N., Lohse, T., Marcowith, A., Martin, J.-M., Martineau-Huynh, O., Masterson, C., McComb, T. J. L., de Naurois, M., Nolan, S. J., Noutsos, A., Orford, K. J., Osborne, J. L., Ouchrif, M., Panter, M., Pelletier, G., Pita, S.,

Pühlhofer, G., Punch, M., Raubenheimer, B. C., Raue, M., Raux, J., Rayner, S. M., Reimer, A., Reimer, O., Ripken, J., Rob, L., Rolland, L., Rowell, G., Sahakian, V., Saugé, L., Schlenker, S., Schlickeiser, R., Schuster, C., Schwanke, U., Siewert, M., Sol, H., Spangler, D., Steenkamp, R., Stegmann, C., Tavernet, J.-P., Terrier, R., Théoret, C. G., Tluczykont, M., Vasileiadis, G., Venter, C., Vincent, P., Völk, H. J., & Wagner, S. J. 2005a. Discovery of Very High Energy Gamma Rays Associated with an X-ray Binary. *Science*, **309**(July), 746–749.

Aharonian, F., Akhperjanian, A. G., Aye, K.-M., Bazer-Bachi, A. R., Beilicke, M., Benbow, W., Berge, D., Berghaus, P., Bernlöhr, K., Bolz, O., Boisson, C., Borgmeier, C., Breitling, F., Brown, A. M., Bussons Gordo, J., Chadwick, P. M., Chitnis, V. R., Chounet, L.-M., Cornils, R., Costamante, L., Degrange, B., Djannati-Ataï, A., Drury, L. O., Ergin, T., Espigat, P., Feinstein, F., Fleury, P., Fontaine, G., Funk, S., Gallant, Y. A., Giebels, B., Gillessen, S., Goret, P., Guy, J., Hadjichristidis, C., Hauser, M., Heinzelmann, G., Henri, G., Hermann, G., Hinton, J. A., Hofmann, W., Holleran, M., Horns, D., de Jager, O. C., Jung I., Khélifi, B., Komin, N., Konopelko, A., Latham, I. J., Le Gallou, R., Lemoine, M., Lemière, A., Leroy, N., Lohse, T., Marcowith, A., Masterson, C., McComb, T. J. L., de Naurois, M., Nolan, S. J., Noutsos, A., Orford, K. J., Osborne, J. L., Ouchrif, M., Panter, M., Pelletier, G., Pita, S., Pohl, M., Pühlhofer, G., Punch, M., Raubenheimer, B. C., Raue, M., Raux, J., Rayner, S. M., Redondo, I., Reimer, A., Reimer, O., Ripken, J., Rivoal, M., Rob, L., Rolland, L., Rowell, G., Sahakian, V., Saugé, L., Schlenker, S., Schlickeiser, R., Schuster, C., Schwanke, U., Siewert, M., Sol, H., Steenkamp, R., Stegmann, C., Tavernet, J.-P., Théoret, C. G., Tluczykont, M., van der Walt, D. J., Vasileiadis, G., Vincent, P., Visser, B., Völk, H. J., & Wagner, S. J. 2005b. H.E.S.S. observations of PKS 2155-304. *Astronomy and Astrophysics*, **430**(Feb.), 865–875.

Albert, J., Aliu, E., Anderhub, H., Antoranz, P., Armada, A., Asensio, M., Baixeras, C., Barrio, J. A., Bartelt, M., Bartko, H., Bastieri, D., Bavikadi, S. R., Bednarek, W., Berger, K., Bigongiari, C., Biland, A., Bisesi, E., Bock, R. K., Bordas, P., Bosch-Ramon, V., Bretz, T., Britvitch, I., Camara, M., Carmona, E., Chilingarian, A., Ciprini, S., Coarasa, J. A., Commichau, S., Contreras, J. L., Cortina, J., Curtef, V., Danielyan, V., Dazzi, F., De Angelis, A., de los Reyes, R., De Lotto, B., Domingo-Santamaría, E., Dorner, D., Doro, M., Errando, M., Fagiolini, M., Ferenc, D., Fernández, E., Firpo, R., Flix, J., Fonseca, M. V., Font, L., Fuchs, M., Galante, N., Garczarczyk, M., Gaug, M., Giller, M., Goebel, F., Hakobyan, D., Hayashida, M., Hengstebeck, T., Höhne, D., Hose, J., Hsu, C. C., Isar, P. G., Jacon, P., Kalekin, O., Kosyra, R., Kranich, D., Laatiaoui, M., Laille, A., Lenisa, T., Liebing, P., Lindfors, E., Lombardi, S., Longo, F., López, J., López, M., Lorenz, E., Lucarelli, F., Majumdar, P., Maneva, G., Mannheim, K., Mansutti, O., Mariotti, M., Martínez, M., Mase, K., Mazin, D., Merck, C., Meucci, M., Meyer, M., Miranda, J. M., Mirzoyan, R., Mizobuchi, S., Moralejo, A., Nilsson, K., Oña-Wilhelmi, E., Orduña, R., Otte, N., Oya, I., Paneque, D., Paoletti, R., Paredes, J. M., Pasanen, M., Pascoli, D., Pauss, F., Pavel, N., Pegna, R., Persic, M., Peruzzo, L., Piccioli, A., Poller, M., Pooley, G., Prandini, E., Raymers, A., Rhode, W., Ribó, M., Rico, J., Riegel, B., Rissi, M., Robert, A., Romero, G. E., Rügamer, S., Saggion, A., Sánchez, A., Sartori, P., Scalzotto, V., Scapin, V., Schmitt, R., Schweizer, T., Shayduk, M., Shinozaki, K., Shore, S. N., Sidro, N., Sillanpää, A., Sobczynska, D., Stamerra, A., Stark, L. S., Takalo, L., Temnikov,

P., Tescaro, D., Teshima, M., Tonello, N., Torres, A., Torres, D. F., Turini, N., Vankov, H., Vitale, V., Wagner, R. M., Wibig, T., Wittek, W., Zanin, R., & Zapatero, J. 2006. Variable Very-High-Energy Gamma-Ray Emission from the Microquasar LS I +61 303. *Science*, **312**(June), 1771–1773.

Audouze, J., & Tinsley, B. M. 1976. Chemical evolution of galaxies. *Annual Review of Astron and Astrophys*, **14**, 43–79.

Baldry, I. K., & Glazebrook, K. 2003. Constraints on a Universal Stellar Initial Mass Function from Ultraviolet to Near-Infrared Galaxy Luminosity Densities. *Astrophysical Journal*, **593**(Aug.), 258–271.

Beacom, J. F. 2010. The Diffuse Supernova Neutrino Background. *Annual Review of Nuclear and Particle Science*, **60**(Nov.), 439–462.

Beichman, C. A., & Helou, G. 1991. What COBE might see - The far-infrared cosmological background. *Astrophysical Journal, Letters*, **370**(Mar.), L1–L4.

Bernstein, R. 2000. *Extragalactic Background Light*. Bristol: Institute of Physics Publishing. Page 2639.

Béthermin, M., Dole, H., Beelen, A., & Aussel, H. 2010. Spitzer deep and wide legacy mid- and far-infrared number counts and lower limits of cosmic infrared background. *Astronomy and Astrophysics*, **512**(Mar.), A78.

Binney, J., & Merrifield, M. 1998. *Galactic Astronomy*. Princeton University Press.

Blain, A. W., & Longair, M. S. 1993. Submillimetre Cosmology. *Monthly Notices of the RAS*, **264**(Sept.), 509.

Blain, A. W., Jameson, A., Smail, I., Longair, M. S., Kneib, J.-P., & Ivison, R. J. 1999. Dust-obscured star formation and AGN fuelling in hierarchical models of galaxy evolution. *Monthly Notices of the RAS*, **309**(Nov.), 715–730.

Bressan, A., Fagotto, F., Bertelli, G., & Chiosi, C. 1993. Evolutionary sequences of stellar models with new radiative opacities. II - Z = 0.02. *Astronomy and Astrophysics, Supplement*, **100**(Sept.), 647–664.

Bruzual, G., & Charlot, S. 2003. Stellar population synthesis at the resolution of 2003. *Monthly Notices of the RAS*, **344**(Oct.), 1000–1028.

Calzetti, D., & Heckman, T. M. 1999. The Evolution of Dust Opacity in Galaxies. *Astrophysical Journal*, **519**(July), 27–47.

Cole, S., Aragon-Salamanca, A., Frenk, C. S., Navarro, J. F., & Zepf, S. E. 1994. A Recipe for Galaxy Formation. *Monthly Notices of the RAS*, **271**(Dec.), 781.

Cole, S., Norberg, P., Baugh, C. M., Frenk, C. S., Bland-Hawthorn, J., Bridges, T., Cannon, R., Colless, M., Collins, C., Couch, W., Cross, N., Dalton, G., De Propris, R., Driver, S. P., Efstathiou, G., Ellis, R. S., Glazebrook, K., Jackson, C., Lahav, O., Lewis, I., Lumsden, S., Maddox, S., Madgwick, D., Peacock, J. A., Peterson, B. A., Sutherland, W., & Taylor, K. 2001. The 2dF galaxy redshift survey: near-infrared galaxy luminosity functions. *Monthly Notices of the RAS*, **326**(Sept.), 255–273.

Condon, J. J., Anderson, M. L., & Helou, G. 1991. Correlations between the far-infrared, radio, and blue luminosities of spiral galaxies. *Astrophysical Journal*, **376**(July), 95–103.

Costamante, L. 2013. Gamma-Rays from Blazars and the Extragalactic Background Light. *International Journal of Modern Physics D*, **22**(Nov.), 30025.

Desert, F.-X., Boulanger, F., & Puget, J. L. 1990. Interstellar dust models for extinction and emission. *Astronomy and Astrophysics*, **237**(Oct.), 215–236.

Devriendt, J. E. G., & Guiderdoni, B. 2000. Galaxy modelling. II. Multi-wavelength faint counts from a semi-analytic model of galaxy formation. *Astronomy and Astrophysics*, **363**(Nov.), 851–862.

Dole, H., Lagache, G., Puget, J.-L., Caputi, K. I., Fernández-Conde, N., Le Floc'h, E., Papovich, C., Pérez-González, P. G., Rieke, G. H., & Blaylock, M. 2006. The cosmic infrared background resolved by Spitzer. Contributions of mid-infrared galaxies to the far-infrared background. *Astronomy and Astrophysics*, **451**(May), 417–429.

Domínguez, A., Primack, J. R., Rosario, D. J., Prada, F., Gilmore, R. C., Faber, S. M., Koo, D. C., Somerville, R. S., Pérez-Torres, M. A., Pérez-González, P., Huang, J.-S., Davis, M., Guhathakurta, P., Barmby, P., Conselice, C. J., Lozano, M., Newman, J. A., & Cooper, M. C. 2011. Extragalactic background light inferred from AEGIS galaxy-SED-type fractions. *Monthly Notices of the RAS*, **410**(Feb.), 2556–2578.

Driver, S. P., Popescu, C. C., Tuffs, R. J., Graham, A. W., Liske, J., & Baldry, I. 2008. The Energy Output of the Universe from 0.1 to 1000 μm. *Astrophysical Journal, Letters*, **678**(May), L101–L104.

Dunne, L., Eales, S., Edmunds, M., Ivison, R., Alexander, P., & Clements, D. L. 2000. The SCUBA Local Universe Galaxy Survey - I. First measurements of the submillimetre luminosity and dust mass functions. *Monthly Notices of the RAS*, **315**(June), 115–139.

Dwek, E. 1998. The Evolution of the Elemental Abundances in the Gas and Dust Phases of the Galaxy. *Astrophysical Journal*, **501**(July), 643.

Dwek, E. 2001 (Jan.). The Role of Dust in Producing the Extragalactic Diffuse Background. *Page 389 of:* Harwit, M., & Hauser, M. G. (eds), *The Extragalactic Infrared Background and its Cosmological Implications*. IAU Symposium, vol. 204.

Dwek, E., & Barker, M. K. 2002. The Cosmic Radio and Infrared Backgrounds Connection. *Astrophysical Journal*, **575**(Aug.), 7–11.

Dwek, E., & Krennrich, F. 2013. The extragalactic background light and the gamma-ray opacity of the universe. *Astroparticle Physics*, **43**(Mar.), 112–133.

Dwek, E., Arendt, R. G., Fixsen, D. J., Sodroski, T. J., Odegard, N., Weiland, J. L., Reach, W. T., Hauser, M. G., Kelsall, T., Moseley, S. H., Silverberg, R. F., Shafer, R. A., Ballester, J., Bazell, D., & Isaacman, R. 1997. Detection and Characterization of Cold Interstellar Dust and Polycyclic Aromatic Hydrocarbon Emission, from COBE Observations. *Astrophysical Journal*, **475**(Feb.), 565–579.

Dwek, E., Arendt, R. G., Hauser, M. G., Fixsen, D., Kelsall, T., Leisawitz, D., Pei, Y. C., Wright, E. L., Mather, J. C., Moseley, S. H., Odegard, N., Shafer, R., Silverberg, R. F., & Weiland, J. L. 1998. The COBE Diffuse Infrared Background Experiment Search for the Cosmic Infrared Background. IV. Cosmological Implications. *Astrophysical Journal*, **508**(Nov.), 106–122.

Dwek, E., Staguhn, J. G., Arendt, R. G., Capak, P. L., Kovacs, A., Benford, D. J., Fixsen, D., Karim, A., Leclercq, S., Maher, S. F., Moseley, S. H., Schinnerer, E., & Sharp, E. H. 2011. Star and Dust Formation Activities in AzTEC-3, a Starburst Galaxy at z = 5.3. *Astrophysical Journal*, **738**(Sept.), 36.

Elbaz, D., Cesarsky, C. J., Chanial, P., Aussel, H., Franceschini, A., Fadda, D., & Chary, R. R. 2002. The bulk of the cosmic infrared background resolved by ISOCAM. *Astronomy and Astrophysics*, **384**(Mar.), 848–865.

Fazio, G. G., Ashby, M. L. N., Barmby, P., Hora, J. L., Huang, J.-S., Pahre, M. A., Wang, Z., Willner, S. P., Arendt, R. G., Moseley, S. H., Brodwin, M., Eisenhardt, P., Stern, D., Tollestrup, E. V., & Wright, E. L. 2004. Number Counts at 3 μm ¡ λ ¡ 10 μm from the Spitzer Space Telescope. *Astrophysical Journal, Supplement*, **154**(Sept.), 39–43.

Finke, J. D., Razzaque, S., & Dermer, C. D. 2010. Modeling the Extragalactic Background Light from Stars and Dust. *The Astrophysical Journal*, **712**(Mar.), 238–249.

Fioc, M., & Rocca-Volmerange, B. 1997. PEGASE: a UV to NIR spectral evolution model of galaxies. Application to the calibration of bright galaxy counts. *Astronomy and Astrophysics*, **326**(Oct.), 950–962.

Fixsen, D. J., Dwek, E., Mather, J. C., Bennett, C. L., & Shafer, R. A. 1998. The Spectrum of the Extragalactic Far-Infrared Background from the COBE FIRAS Observations. *Astrophysical Journal*, **508**(Nov.), 123–128.

Fontanot, F., & Somerville, R. S. 2011. Evaluating and improving semi-analytic modelling of dust in galaxies based on radiative transfer calculations - II. Dust emission in the infrared. *Monthly Notices of the RAS*, **416**(Oct.), 2962–2973.

Fontanot, F., Somerville, R. S., Silva, L., Monaco, P., & Skibba, R. 2009. Evaluating and improving semi-analytic modelling of dust in galaxies based on radiative transfer calculations. *Monthly Notices of the RAS*, **392**(Jan.), 553–569.

Franceschini, A., Mazzei, P., de Zotti, G., & Danese, L. 1994. Luminosity evolution and dust effects in distant galaxies: Implications for the observability of the early evolutionary phases. *Astrophysical Journal*, **427**(May), 140–154.

Franceschini, A., Elbaz, D., Fadda, D., & Cesarsky, C. J. 2002. The AGN Contribution to the Cosmic Infrared Background: Steps towards Measuring the Gravitational vs. Stellar Global Energy Budget. *Page 229 of:* Maiolino, R., Marconi, A., & Nagar, N. (eds), *Issues in Unification of Active Galactic Nuclei*. Astronomical Society of the Pacific Conference Series, vol. 258.

Franceschini, A., Rodighiero, G., & Vaccari, M. 2008. Extragalactic optical-infrared background radiation, its time evolution and the cosmic photon-photon opacity. *Astronomy and Astrophysics*, **487**(Sept.), 837–852.

Furniss, A., Sutter, P. M., Primack, J. R., & Domínguez, A. 2015. A correlation between hard gamma-ray sources and cosmic voids along the line of sight. *Monthly Notices of the RAS*, **446**(Jan.), 2267–2273.

Gilmore, R. C., Somerville, R. S., Primack, J. R., & Domínguez, A. 2012. Semi-analytic modelling of the extragalactic background light and consequences for extragalactic gamma-ray spectra. *Monthly Notices of the Royal Astronomical Society*, **422**(June), 3189–3207.

Gordon, K. D., Misselt, K. A., Witt, A. N., & Clayton, G. C. 2001. The DIRTY Model. I. Monte Carlo Radiative Transfer through Dust. *Astrophysical Journal*, **551**(Apr.), 269–276.

Gould, R. J., & Schréder, G. P. 1967. Pair Production in Photon-Photon Collisions. *Physical Review*, **155**(Mar.), 1404–1407.

Guo, Q., White, S., Angulo, R. E., Henriques, B., Lemson, G., Boylan-Kolchin, M., Thomas, P., & Short, C. 2013. Galaxy formation in WMAP1 and WMAP7 cosmologies. *Monthly Notices of the RAS*, **428**(Jan.), 1351–1365.

Haarsma, D. B., & Partridge, R. B. 1998. Radio Wavelength Constraints on the Sources of the Far-Infrared Background. *Astrophysical Journal, Letters*, **503**(Aug.), L5–L8.

Hacking, P. B., & Soifer, B. T. 1991. The number counts and infrared backgrounds from infrared-bright galaxies. *Astrophysical Journal, Letters*, **367**(Feb.), L49–L53.

Hainline, L. J., Blain, A. W., Smail, I., Frayer, D. T., Chapman, S. C., Ivison, R. J., & Alexander, D. M. 2009. A Mid-Infrared Imaging Survey of Submillimeter-Selected Galaxies with the Spitzer Space Telescope. *Astrophysical Journal*, **699**(July), 1610–1632.

Hauser, M. G., & Dwek, E. 2001. The Cosmic Infrared Background: Measurements and Implications. *Annual Review of Astronomy and Astrophysics*, **39**, 249–307.

Hauser, M. G., Arendt, R. G., Kelsall, T., Dwek, E., Odegard, N., Weiland, J. L., Freudenreich, H. T., Reach, W. T., Silverberg, R. F., Moseley, S. H., Pei, Y. C., Lubin, P., Mather, J. C., Shafer, R. A., Smoot, G. F., Weiss, R., Wilkinson, D. T., & Wright, E. L. 1998. The COBE Diffuse Infrared Background Experiment Search for the Cosmic Infrared Background. I. Limits and Detections. *Astrophysical Journal*, **508**(Nov.), 25–43.

Helgason, K., & Kashlinsky, A. 2012. Reconstructing the γ-Ray Photon Optical Depth of the Universe to z ˜ 4 from Multiwavelength Galaxy Survey Data. *Astrophysical Journal, Letters*, **758**(Oct.), L13.

Hopkins, A. M., & Beacom, J. F. 2006. On the Normalization of the Cosmic Star Formation History. *Astrophysical Journal*, **651**(Nov.), 142–154.

Horiuchi, S., Beacom, J. F., & Dwek, E. 2009. Diffuse supernova neutrino background is detectable in Super-Kamiokande. *Physical Review D*, **79**(8), 083013.

Jackson, John David. 1998. *Classical Electrodynamics Third Edition*. 3 edn. Wiley.

Jones, D. H., Saunders, W., Colless, M., Read, M. A., Parker, Q. A., Watson, F. G., Campbell, L. A., Burkey, D., Mauch, T., Moore, L., Hartley, M., Cass, P., James, D., Russell, K., Fiegert, K., Dawe, J., Huchra, J., Jarrett, T., Lahav, O., Lucey, J., Mamon, G. A., Proust, D., Sadler, E. M., & Wakamatsu, K.-i. 2004. The 6dF Galaxy Survey: samples, observational techniques and the first data release. *Monthly Notices of the RAS*, **355**(Dec.), 747–763.

Kashlinsky, A. 2005. Cosmic infrared background and early galaxy evolution [review article]. *Physics Reports*, **409**(Apr.), 361–438.

Kashlinsky, A., Mather, J. C., Odenwald, S., & Hauser, M. G. 1996a. Clustering of DIRBE Light and IR Background. *Pages 115–121 of:* Dwek, E. (ed), *American Institute of Physics Conference Series*. American Institute of Physics Conference Series, vol. 348.

Kashlinsky, A., Mather, J. C., & Odenwald, S. 1996b. Clustering of the Diffuse Infrared Light from the COBE DIRBE Maps: an All-Sky Survey of C(0). *Astrophysical Journal, Letters*, **473**(Dec.), L9.

Kashlinsky, A., Mather, J. C., Odenwald, S., & Hauser, M. G. 1996c. Clustering of the Diffuse Infrared Light from the COBE DIRBE Maps. I. C(0) and Limits on the Near-Infrared Background. *Astrophysical Journal*, **470**(Oct.), 681.

Kauffmann, G., White, S. D. M., & Guiderdoni, B. 1993. The Formation and Evolution of Galaxies Within Merging Dark Matter Haloes. *Monthly Notices of the RAS*, **264**(Sept.), 201.

Kelsall, T., Weiland, J. L., Franz, B. A., Reach, W. T., Arendt, R. G., Dwek, E., Freudenreich, H. T., Hauser, M. G., Moseley, S. H., Odegard, N. P., Silverberg, R. F., & Wright, E. L. 1998. The COBE Diffuse Infrared Background Experiment Search for the Cosmic Infrared Background. II. Model of the Interplanetary Dust Cloud. *Astrophysical Journal*, **508**(Nov.), 44–73.

Lagache, G., & Puget, J. L. 2000. Detection of the extra-Galactic background fluctuations at 170 mu m. *Astronomy and Astrophysics*, **355**(Mar.), 17–22.

Lagache, G., Dole, H., & Puget, J.-L. 2003. Modelling infrared galaxy evolution using a phenomenological approach. *Monthly Notices of the RAS*, **338**(Jan.), 555–571.

Leitherer, C., Schaerer, D., Goldader, J. D., Delgado, R. M. G., Robert, C., Kune, D. F., de Mello, D. F., Devost, D., & Heckman, T. M. 1999. Starburst99: Synthesis Models for Galaxies with Active Star Formation. *Astrophysical Journal, Supplement*, **123**(July), 3–40.

Lemson, G., & Virgo Consortium, t. 2006. Halo and Galaxy Formation Histories from the Millennium Simulation: Public release of a VO-oriented and SQL-queryable database for studying the evolution of galaxies in the LambdaCDM cosmogony. *ArXiv Astrophysics e-prints*, Aug.

Lisenfeld, U., Voelk, H. J., & Xu, C. 1996. A quantitative model of the FIR/radio correlation for normal late-type galaxies. *Astronomy and Astrophysics*, **306**(Feb.), 677.

Madau, P., & Pozzetti, L. 2000. Deep galaxy counts, extragalactic background light and the stellar baryon budget. *Monthly Notices of the RAS*, **312**(Feb.), L9–L15.

Malkan, M. A., & Stecker, F. W. 1998. An Empirically Based Calculation of the Extragalactic Infrared Background. *Astrophysical Journal*, **496**(Mar.), 13–16.

Malkan, M. A., & Stecker, F. W. 2001. An Empirically Based Model for Predicting Infrared Luminosity Functions, Deep Infrared Galaxy Counts, and the Diffuse Infrared Background. *Astrophysical Journal*, **555**(July), 641–649.

Malkov, M. A., & O'C Drury, L. 2001. Nonlinear theory of diffusive acceleration of particles by shock waves. *Reports on Progress in Physics*, **64**(Apr.), 429–481.

Maraston, C., & Strömbäck, G. 2011. Stellar population models at high spectral resolution. *Monthly Notices of the RAS*, **418**(Dec.), 2785–2811.

Mazin, D., & Raue, M. 2007. New limits on the density of the extragalactic background light in the optical to the far infrared from the spectra of all known TeV blazars. *Astronomy and Astrophysics*, **471**(Aug.), 439–452.

Mushotzky, R. F., Cowie, L. L., Barger, A. J., & Arnaud, K. A. 2000. Resolving the extragalactic hard X-ray background. *Nature*, **404**(Mar.), 459–464.

Nenkova, M., Ivezić, Ž., & Elitzur, M. 2000. DUSTY: a Publicly Available Code for Modeling Dust Emission. *Thermal Emission Spectroscopy and Analysis of Dust, Disks, and Regoliths*, **196**(Mar.), 77–82.

Omukai, K., Tsuribe, T., Schneider, R., & Ferrara, A. 2005. Thermal and Fragmentation Properties of Star-forming Clouds in Low-Metallicity Environments. *Astrophysical Journal*, **626**(June), 627–643.

Orr, M. R., Krennrich, F., & Dwek, E. 2011. Strong New Constraints on the Extragalactic Background Light in the Near- to Mid-infrared. *Astrophysical Journal*, **733**(June), 77.

Pagel, B. E. J. 2001. Chemical Evolution of Galaxies. *Publications of the ASP*, **113**(Feb.), 137–141.

Pei, Y. C., Fall, S. M., & Hauser, M. G. 1999. Cosmic Histories of Stars, Gas, Heavy Elements, and Dust in Galaxies. *Astrophysical Journal*, **522**(Sept.), 604–626.

Pénin, A., Lagache, G., Noriega-Crespo, A., Grain, J., Miville-Deschênes, M.-A., Ponthieu, N., Martin, P., Blagrave, K., & Lockman, F. J. 2012. An accurate measurement of the anisotropies and mean level of the cosmic infrared background at 100 μm and 160 μm. *Astronomy and Astrophysics*, **543**(July), A123.

Ponente, P. P., Ascasibar, Y., & Diego, J. M. 2011. The contribution of star-forming galaxies to the cosmic radio background. *Monthly Notices of the RAS*, **418**(Nov.), 691–695.

Prialnik, Dina. 2000. *An introduction to the theory of stellar structure and evolution.* Cambridge University Press.

Primack, J. R., Bullock, J. S., Somerville, R. S., & MacMinn, D. 1999. Probing galaxy formation with TeV gamma ray absorption. *Astroparticle Physics*, **11**(June), 93–102.

Primack, J. R., Bullock, J. S., & Somerville, R. S. 2005 (Feb.). Observational Gamma-ray Cosmology. *Pages 23–33 of:* Aharonian, F. A., Völk, H. J., & Horns, D. (eds), *High Energy Gamma-Ray Astronomy.* American Institute of Physics Conference Series, vol. 745.

Punch, M., Akerlof, C. W., Cawley, M. F., Chantell, M., Fegan, D. J., Fennell, S., Gaidos, J. A., Hagan, J., Hillas, A. M., Jiang, Y., Kerrick, A. D., Lamb, R. C., Lawrence, M. A., Lewis, D. A., Meyer, D. I., Mohanty, G., O'Flaherty, K. S., Reynolds, P. T., Rovero, A. C., Schubnell, M. S., Sembroski, G., Weekes, T. C., & Wilson, C. 1992. Detection of TeV photons from the active galaxy Markarian 421. *Nature*, **358**(Aug.), 477.

Razzaque, S., Dermer, C. D., & Finke, J. D. 2009. The Stellar Contribution to the Extragalactic Background Light and Absorption of High-Energy Gamma Rays. *The Astrophysical Journal*, **697**(May), 483–492.

Rodighiero, G., Vaccari, M., Franceschini, A., Tresse, L., Le Fevre, O., Le Brun, V., Mancini, C., Matute, I., Cimatti, A., Marchetti, L., Ilbert, O., Arnouts, S., Bolzonella, M., Zucca, E., Bardelli, S., Lonsdale, C. J., Shupe, D., Surace, J., Rowan-Robinson, M., Garilli, B., Zamorani, G., Pozzetti, L., Bondi, M., de la Torre, S., Vergani, D., Santini, P., Grazian, A., & Fontana, A. 2010. Mid- and far-infrared luminosity functions and galaxy evolution from multiwavelength Spitzer observations up to z ˜ 2.5. *Astronomy and Astrophysics*, **515**(June), A8.

Rowan-Robinson, M. 2001. Models for the IR and submm SEDs of normal, starburst and active galaxies. *New Astronomy Review*, **45**(Oct.), 631–639.

Rowan-Robinson, M. 2009. A new model for infrared and submillimetre counts. *Monthly Notices of the RAS*, **394**(Mar.), 117–123.

Ruderman, M. A., & Sutherland, P. G. 1975. Theory of pulsars - Polar caps, sparks, and coherent microwave radiation. *Astrophysical Journal*, **196**(Feb.), 51–72.

Salpeter, E. E. 1955. The Luminosity Function and Stellar Evolution. *Astrophysical Journal*, **121**(Jan.), 161.

Scalo, J. 1998. The IMF Revisited: A Case for Variations. *Page 201 of:* Gilmore, G., & Howell, D. (eds), *The Stellar Initial Mass Function (38th Herstmonceux Conference).* Astronomical Society of the Pacific Conference Series, vol. 142.

Scalo, J. M. 1986. The stellar initial mass function. *Fundamental Cosmic Physics*, **11**(May), 1–278.

Schneider, R. 2006. Constraining the epoch of very massive star formation. *New Astronomy Review*, **50**(Mar.), 64–69.

Schönfelder, Volker. 2001. *The Universe in Gamma Rays*. Astronomy and Astrophysics Library. Springer Berlin Heidelberg.

Shectman, S. A. 1973. Clusters of Galaxies and the Cosmic Light. *Astrophysical Journal*, **179**(Feb.), 681–698.

Shectman, S. A. 1974. The small-scale anisotropy of the cosmic light. *Astrophysical Journal*, **188**(Mar.), 233–242.

Silva, L., Granato, G. L., Bressan, A., & Danese, L. 1998. Modeling the Effects of Dust on Galactic Spectral Energy Distributions from the Ultraviolet to the Millimeter Band. *Astrophysical Journal*, **509**(Dec.), 103–117.

Skrutskie, M. F., Cutri, R. M., Stiening, R., Weinberg, M. D., Schneider, S., Carpenter, J. M., Beichman, C., Capps, R., Chester, T., Elias, J., Huchra, J., Liebert, J., Lonsdale, C., Monet, D. G., Price, S., Seitzer, P., Jarrett, T., Kirkpatrick, J. D., Gizis, J. E., Howard, E., Evans, T., Fowler, J., Fullmer, L., Hurt, R., Light, R., Kopan, E. L., Marsh, K. A., McCallon, H. L., Tam, R., Van Dyk, S., & Wheelock, S. 2006. The Two Micron All Sky Survey (2MASS). *Astronomical Journal*, **131**(Feb.), 1163–1183.

Soifer, B. T., Helou, G., & Werner, M. 2008. The Spitzer View of the Extragalactic Universe. *Annual Review of Astron and Astrophys*, **46**(Sept.), 201–240.

Somerville, R. S., & Primack, J. R. 1999. Semi-analytic modelling of galaxy formation: the local Universe. *Monthly Notices of the RAS*, **310**(Dec.), 1087–1110.

Spergel, D. N., Bean, R., Doré, O., Nolta, M. R., Bennett, C. L., Dunkley, J., Hinshaw, G., Jarosik, N., Komatsu, E., Page, L., Peiris, H. V., Verde, L., Halpern, M., Hill, R. S., Kogut, A., Limon, M., Meyer, S. S., Odegard, N., Tucker, G. S., Weiland, J. L., Wollack, E., & Wright, E. L. 2007. Three-Year Wilkinson Microwave Anisotropy Probe (WMAP) Observations: Implications for Cosmology. *Astrophysical Journal, Supplement*, **170**(June), 377–408.

Stecker, F. W., Malkan, M. A., & Scully, S. T. 2006. Intergalactic Photon Spectra from the Far-IR to the UV Lyman Limit for 0 ¡ z ¡ 6 and the Optical Depth of the Universe to High-Energy Gamma Rays. *Astrophysical Journal*, **648**(Sept.), 774–783.

Tan, J. C., Silk, J., & Balland, C. 1999. A Semiempirical Model of the Infrared Universe. *Astrophysical Journal*, **522**(Sept.), 579–589.

Tinsley, B. M. 1981. Chemical evolution in the solar neighborhood. IV - Some revised general equations and a specific model. *Astrophysical Journal*, **250**(Nov.), 758–768.

Treister, E., Urry, C. M., Van Duyne, J., Dickinson, M., Chary, R.-R., Alexander, D. M., Bauer, F., Natarajan, P., Lira, P., & Grogin, N. A. 2006. Spitzer Number Counts of Active Galactic Nuclei in the GOODS Fields. *Astrophysical Journal*, **640**(Apr.), 603–611.

VERITAS Collaboration, Acciari, V. A., Aliu, E., Arlen, T., Aune, T., Bautista, M., Beilicke, M., Benbow, W., Boltuch, D., Bradbury, S. M., Buckley, J. H., Bugaev, V., Byrum, K., Cannon, A., Celik, O., Cesarini, A., Chow, Y. C., Ciupik, L., Cogan, P., Colin, P., Cui, W., Dickherber, R., Duke, C., Fegan, S. J., Finley, J. P., Finnegan, G., Fortin, P., Fortson, L., Furniss, A., Galante, N., Gall, D., Gibbs, K., Gillanders, G. H., Godambe, S., Grube, J., Guenette, R., Gyuk, G., Hanna, D., Holder, J., Horan, D., Hui, C. M., Humensky, T. B., Imran, A., Kaaret, P., Karlsson, N., Kertzman, M., Kieda, D., Kildea, J., Konopelko, A., Krawczynski, H., Krennrich, F., Lang, M. J., Lebohec, S., Maier, G., McArthur, S., McCann, A., McCutcheon, M., Millis, J., Moriarty, P., Mukherjee, R., Nagai, T., Ong, R. A., Otte, A. N., Pandel, D., Perkins, J. S., Pizlo, F., Pohl, M., Quinn, J., Ragan, K., Reyes, L. C., Reynolds, P. T., Roache, E., Rose, H. J., Schroedter, M., Sembroski, G. H., Smith, A. W., Steele, D., Swordy, S. P., Theiling, M., Thibadeau, S., Varlotta, A., Vassiliev, V. V., Vincent, S., Wagner, R. G., Wakely, S. P., Ward, J. E., Weekes, T. C., Weinstein, A., Weisgarber, T., Williams, D. A., Wissel, S., Wood, M., & Zitzer, B. 2009. A connection between star formation activity and cosmic rays in the starburst galaxy M82. *Nature*, **462**(Dec.), 770–772.

Vogeley, M. S. 1997. Fluctuations in the Extragalactic Background Light: Analysis of the Hubble Deep Field. *ArXiv Astrophysics e-prints*, Nov.

Weekes, T. (ed). 2003 (Apr.). *Very High Energy Gamma-Ray Astronomy*. Wiley Praxis Series in Astronomy and Astrophysics, vol. 11.

Xu, C. 2000. Local Luminosity Function at 15 Microns and Galaxy Evolution Seen by ISOCAM 15 Micron Surveys. *Astrophysical Journal*, **541**(Sept.), 134–141.

Yoshii, Y., & Takahara, F. 1988. Galactic evolution and cosmology - Probing the cosmological deceleration parameter. *Astrophysical Journal*, **326**(Mar.), 1–18.

Younger, J. D., & Hopkins, P. F. 2011. A physical model for the origin of the diffuse cosmic infrared background and the opacity of the Universe to very high energy γ-rays. *Monthly Notices of the RAS*, **410**(Feb.), 2180–2192.

Yuan, Q., Huang, H.-L., Bi, X.-J., & Zhang, H.-H. 2012. Measuring the extragalactic background light from very high energy gamma-ray observations of blazars. *ArXiv e-prints*, Dec.